THE EFFECTS OF INCREASED CAMP LEVELS ON NEURONAL DIFFERENTIATION IN MURINE EMBRYONIC STEM CELLS, AND THE CREATION OF A CRISPR-INDUCED C.1252C>T POINT MUTATION IN THE ADCY5 GENE

By

Elizabeth Zepeda

A Thesis Presented to

The Faculty of Humboldt State University

In Partial Fulfillment of the Requirements for the Degree

Master of Science in Biology

Committee Membership

Dr. Amy Sprowles, Committee Chair

Dr. Christina Waters, Committee Member

Dr. Bruce O'Gara, Committee Member

Dr. John Steele, Committee Member

Dr. Erik S. Jules, Program Graduate Coordinator

December 2018

ABSTRACT

THE EFFECTS OF INCREASED CAMP LEVELS ON NEURONAL DIFFERENTIATION IN MURINE EMBRYONIC STEM CELLS, AND THE CREATION OF A CRISPR-INDUCED C.1252C>T POINT MUTATION IN THE ADCY5 GENE

Elizabeth Zepeda

ADCY5-related dyskinesia is a rare movement disorder with early onset in childhood and adolescence. Previous studies linked this disease to various point mutations in the ADCY5 gene. Recent studies show that two of the point mutations cause an increase in cyclic adenosine monophosphate (cAMP) levels. However, it remains unknown how increased levels of cAMP result in the phenotypes associated with this disease. My study examines the effects of increased cAMP levels on neuronal differentiation of mouse embryonic stem cells (mESCs). My experiments demonstrated successful differentiation of mESCs into the dopaminergic neuronal lineage, indicated by the presence of Tuj 1 (a class III beta-tubulin neuronal cell marker), and tyrosine hydroxylase (TH) (an enzyme found in dopaminergic neurons), as detected by immunocytochemistry (ICC). To determine the effect of cAMP on this process, murine embryonic stem cells were differentiated in the presence of a range of db-cAMP concentrations. Cells treated with 700 μM of db-cAMP during the differentiation step of the protocol showed increased percentage of the neuronal cell-type, followed by a decrease in percent neuronal-cell type treated with 1400 μM and 2800 μM db-cAMP.

There was no significant effect of db-cAMP on percent dopamine-containing neurons. In addition, there were lower levels of tyrosine hydroxylase (TH) protein present in the membrane fraction, in cells treated with 1400 μM db-cAMP compared to no treatment, and no significant change in cytosolic TH. My results also revealed an increase in dopamine receptor D2 in both the membrane and cytosol. In order to characterize the effects of the point mutation p.R418W on cellular cAMP levels in HEK293T cells, I attempted to create a mutation in a HEK293T cell line using CRISPR. Once the mutant cell line was generated, the plan was to treat with pharmacological agonists to beta-adrenergic receptors to stimulate cAMP production in mutated cells as well as control cells. The amount of cAMP produced in mutated cells versus wild-type would then be quantified using enzyme-linked immunosorbent assay (ELISA). After the first round, CRISPR failed to produce the desired mutation, the guide RNA was modified, and the process repeated three times. Although we successfully created the desired edit in the third round, other mutations directly flanking upstream and downstream predicted that ADCY5 protein would be non-functional, so the ELISA was not performed. Overall our results provide a model of the molecular basis of ADCY5 related-dyskinesia, such that high levels of cAMP during early development decreases neuronal cell-type production, as well as exerting its downstream effects on D2 (dopamine 2) receptor and tyrosine hydroxylase protein expression, thereby disrupting the dopamine pathway. Understanding the pathophysiological mechanisms underlying this disease will help differentiate ADCY5 related-dyskinesia from other motor disorders, in order for clinicians to make informed decisions about treatment. Future steps will include the use of patient iPSCs to

individually diagnose mutation type, quantify cAMP production level, and customize drug treatment.

ACKNOWLEDGEMENTS

I would like to thank first and foremost my advisor, Dr. Amy Sprowles, whose guidance throughout this whole process has been indispensable. Her mentorship has harnessed my love of science into new research abilities within my field of interest and sharpened my critical thinking skills. Thank you to my committee members, Dr. Bruce O'Gara, Dr. John Steele, and Dr. Erik Jules, for their consistent mentorship and support throughout this process. A special thanks to our project collaborator and my committee member, Dr. Christina Waters for her willingness to collaborate with students here at Humboldt State University, and her dedication to finding better treatments for rare diseases such as ADCY5-related dyskinesia. Thank you to my fellow graduate students for your assistance and encouragement. I am grateful to my large team of undergraduates, especially Linh Pham, Marco Gonzalez, Kiana Robertson, and Nick Zuniga, who have helped throughout the past two years on this project. Their efforts and hard work have made this research truly come together. This study was funded through the HSU CIRM Bridges Training Grant TB1-01190.

TABLE OF CONTENTS

Field Code Changed

Deleted: Error! Hyperlink reference not valid.List of appendices - xiv

Field Code Changed

Field Code Changed

Deleted: Error! Hyperlink reference not valid.Appendices 82

LIST OF TABLES

LIST OF FIGURES

LIST OF APPENDICES

INTRODUCTION

ADCY5-related dyskinesia is a rare genetic neurological movement disorder, with early onset in childhood (Mencacci et al. 2015). Although this disease is not fatal and does not progress with age (Fernandez et al. 2001), the effects are challenging and debilitating for patients and their families. The disease phenotype was first described in 2001, when Dr. Magali Fernandez and colleagues performed a study on 18 related individuals (spanning over five generations) diagnosed with "some variation" of benign hereditary chorea (BHC). Case workup, including family history, revealed that patients did not continue to deteriorate as in Huntington's disease, and in some cases, there seemed to be improvement with age. Patients' conditions seemed to be worsened by anxiety and stress. There were no marked abnormalities in blood chemistries reported, cognitive dysfunction, or shortened life span; MRI's were normal, deep tendon reflexes were normal, and muscle strength and tone were all normal. Needle electromyogram (EMG) recordings were used to measure patients' facial muscle electrical activity which displayed myokymic electrical discharges. The disease was re-named to Familial dyskinesia with Facial Myokymia (FDFM) due to the various dyskinesias and myokymic presentation. FDFM differs from BHC in the way it clinically presents, such that BHC often presents with pulmonary and or endocrine defects and FDFM does not. Also, BHC's predominant symptom is chorea, and although FDFM does manifest with the neurological-related chorea, it also presents with other multiple abnormal movements, including facial myokymia, dystonia, hypotonia, myoclonus, dysarthria, paroxysmal

episodes, as well as delayed developmental milestones, with early onset in childhood to adolescence (Fernandez et al. 2001).

In order to analyze the genetic basis of this disease, Fernandez et al. 2001 examined the family pedigree of the five-generation family study and discovered the mode of inheritance to be autosomal dominant, with complete penetrance in males and females; and some cases revealed male to male transmission. The authors proposed that the gene mutation responsible for FDFM was most likely related to an ion channel due to some patients' positive response to propranolol, a beta-adrenergic antagonist, as well as acetazolamide, an inhibitor of carbonic anhydrase. They performed linkage analysis on fourteen genomic regions containing genes that code for portions of ligand-gated ion channels in addition to genes associated with myokymia or chorea, but it was not informative (LOD score of 2.7, below the significance level of 3.0). A haplotype analysis was constructed from haplotypes of living affected family members. They found that many affected individuals did not share the haplotype with their affected siblings, or even affected relative. They also demonstrated that FDFM is not an allelic variant of any of the candidate genes examined.

The first exome sequencing of a FDFM affected individual was performed in 2012 by Che, et al. The disorder was mapped to a region on chromosome 3 that contained a missense mutation in the coding sequence for Adenylate Cyclase 5 (ADCY5). Since this discovery, a total of 89 patients presenting with symptoms of FDFM have tested positive for a mutation in the ADCY5 gene (Table 1). These individuals include related family members, as well as non-related sporadic cases, and includes an array of genotype

to phenotype relationship. (Chen, et al. 2012; Chen, et al. 2014; Carapito et al. 2015; Chen, et al. 2015; Douglas et al. 2017; Dy et al. 2015; Menacci et al. 2015; Chang et al. 2016). According to my most current literature search, there are 17 identified ADCY5 point mutations associated with diseased individuals (Douglas et al 2017), as well as one amino acid deletion mutation, for a total of 18 identified ADCY5 mutations associated with the disease (Table 1). The p.R418W mutation in ADCY5 is carried by the majority of ADCY5 patients examined to date and is associated with the more severe phenotypes (Chen, D. et al. 2015; Zech et al. 2017).

The ADCY5 gene is 173,250 bp long and contains 21 exons located on the q arm of chromosome 3 (reviewed in Shaw 2015). The coding sequence is 3,786 bp long, encoding 1,262 amino acids (National Center for Biotechnology Information [updated 2018]). ADCY5 has two identified splice variants that contain the first half of the molecule identified by BLAST analysis against EST databases. The first ADCY5 variant ends at domain C1a, and the second variant ends at the beginning of C2. This has been found similar to the truncated ADCY5 molecule found in cDNA libraries made from canine ventricular tissue. Though inactive on their own, it is hypothesized that the truncated isoforms may allow for heterodimerization *in vivo* (Katsushika et al. 1992).

ADCY5 is one of the 9 transmembrane human adenylate cyclase proteins expressed from the adenylate cyclase genes conserved in all mammals. There is also a 10^{th} ADCY protein that is soluble, structurally different from the others and is testis specific (Chen et al. 2012; reviewed in Dessauer et al. 2017). ADCY5 encodes for a plasma membrane-bound glycoprotein that is an effector enzyme of G-protein coupled

Deleted:

receptors (GPCRs). (Ludwig and Seuwen 2002). The ADCY 5 protein is grouped into adenylate cyclase category III (reviewed in Dessauer et al. 2017), which is defined due to inhibition by Ca^{2+}, PKA, and Gαi subunit and activation by forskolin, isoproterenol, PKC, Gαs & G$\beta\gamma$ subunits, and Mn^{2+} (reviewed in Hurley 1999).

The enzymatic role of adenylate cyclase is the conversion of adenosine triphosphate (ATP) to cyclic adenosine-3',5'- monophosphate and pyrophosphate. Once cAMP is synthesized, it serves as a second messenger within the cell. Cyclic AMP's most prominent role is to phosphorylate cAMP-dependent protein kinase (PKA), which in turn can phosphorylate other molecules causing a wide array of downstream signaling cascade effects, including inhibition of ADCY5 in circuit (Dunman and Nestler 1999). A common role for PKA is the phosphorylation of the transcription factor cAMP response element binding protein (CREB). Phosphoactive CREB translocates to the nucleus where it binds the DNA sequence known as cAMP response element (CRE) to regulate the expression of a variety of genes that include some involved in neural cell function such as BDNF, NGF, and PACAP (Dworkin et al. 2009).

The transmembrane ADCY proteins have two transmembrane domains (TM1 and TM2), each comprised of 6 transmembrane helices each and two cytosolic catalytic domains (C1 and C2). The two catalytic domains have an "a" and "b" subunit. C1 is connected to TM1 and C2 is connected to TM2. Residues of both C1a and C2 come together in a heterodimer to form the active site at one end of the ventral groove (Willoughby and Cooper 2007). The active site of this enzyme is lined with hydrophobic residues allowing for hydrophobic interactions to cradle the purine ring of ATP. The

arginine residue of C1 and the lysine residue of C2 form the charged interactions of the catalytic domain. The C1 domain helps to correctly orient the lysine residue in C2, which in turn is necessary for the flexibility of the active site. Any mutation that changes the specific amino acid residues located within this catalytic site may affect the specificity by preventing proper interaction between C1 and C2 (reviewed in Hurley 1999).

In humans, ADCY5 is predominantly expressed in the striatum (Matsuoka et al. 1997; Kim et al. 2006; Menacci et al. 2013). The dorsal striatum includes the caudate nucleus and putamen, and the ventral striatum includes the nucleus accumbens olfactory tubercles (Figure 1), both dorsal and ventral subsections make up the basal ganglia, subcortical structures involved in movement, learning, and memory (reviewed in Money and Stanwood 2018). In particular, the nigrostriatal pathway of the basal ganglia has a role in controlling voluntary muscle movement. A study demonstrated that ADCY5 mRNA expression continues to increase in the human striatum during early development, from 50 to 500 days post conception, when compared to other regions such as hippocampus, frontal cortex, or medulla oblongata (Menacci et al. 2015). This indicates that the level of ADCY5 expression is associated with early development, in a temporal-spatial manner.

A study by Matsuoka et al 1997 used neonatal and adult rat brain to research mRNA expression of ADCY1, 2, and 5. They found ADCY5 was restricted to striatum, nucleus accumbens, and olfactory tubercle. There was low ADCY5 mRNA expression in these regions in the neonatal rat brain, then a significant increase in these same regions after postnatal day(?) 7. Expression of ADCY5 mRNA is also associated with the

maturation of striatal neurons, while ADCY2 is more distributed throughout the adult rat brain and ADCY1 is abundant in the dentate gyrus of the adult rat brain. The results of their entire study show that ADCY protein 1, 2, and 5 expression is brain region specific, as well as age specific, which they concluded that these specific proteins may have a role, "not only in the synaptic transmission, but also in the differentiation and maturation of neuronal cells in the developing brain" (Matsuoka et al. 1997).

ADCY5 expression has also been characterized in other human tissues. In 2002, Ludwig and Seuwen performed a study in which ADCY expression profiles were created using 16 different tissues from human as well as HEK 293T cells. Using RT-PCR, they found ADCY5 expressed in 14 of the 16 different tissue types, with highest expression in heart, brain, and testes. In HEK 293T cells, cDNA expression of most adenylate cyclase proteins was found, except 4, and 8; and 2 was faintly detectable. A band of moderate intensity for ADCY5 was detected at 300bp (as reviewed in Ludwig and Seuwen 2002). Later, expression of ADCY proteins 1, 3, 4, 5, 6, 7, and 9 was confirmed in HEK 293T cells (Atwood et al. 2011).

Interestingly, all the mutations identified in ADCY5 patients occur within the catalytic domains of the protein (Chen, et al 2015; Chang et al. 2016; Douglas et al. 2017; Dy et al 2016).) (Figure 2). To determine how these mutations might affect biochemical function, a significant study performed in 2014 by Ying-Zhang Chen and colleagues at the University of Washington concluded that the FDFM phenotype may be due to a gain-of function effect due to a mutation found in the adenylate cyclase 5 gene. HEK 293T cells were transiently transfected with either an empty GFP expression vector, GFP

vector + wild-type ADCY5, or GFP vector encoding two mutations identified in ADCY5 patients: p.R418W, or p.A726T. They then measured subsequent cAMP production in the basal state and under pharmacological regulation by the ADCY class III beta adrenergic agonists forskolin and isoproterenol, and the ADCY antagonist, propranolol. ADCY5 protein levels were not affected by the mutations; however, cAMP levels in mutated ADCY5 were significantly higher than basal levels but only when stimulated by pharmacologics, demonstrating a gain-of-function effect. This suggested increased cAMP could be related to disease phenotype in patients carrying these mutations. (Chen, YZ. et al. 2014). They performed whole exome sequencing on affected individuals and discovered several missense variants within the ADCY5 gene. Of note, one of those variants, includes (c.1252C>T, p.R418W), which is of interest for our study. They also mapped these mutations to the catalytic domains of ADCY5.

To date, there is not a solid understanding of the molecular mechanisms by which ADCY5 mutations result in the disease phenotypes. However, there is evidence in the literature to suggest that neuronal differentiation might be affected. Production of cAMP by ADCY5 affects axon elongation, through the P13-Akt-GSK3 pathway. (Puerto, et al. 2012). Specifically, the three purinergic receptors P2X7, P2Y1, P2Y13, widely expressed in neurons and glial cells of the adult brain, contribute to the regulation of ADCY5. The metabotropic receptor P2Y1, promotes axonal elongation through activating cAMP production in the distal region of axons of hippocampal neurons, exerting its effects on downstream effectors that include neurotrophic factors. The P2X7 and P2Y1 receptors halt axonal elongation by inhibiting cAMP synthesis(?) through induction of Ca^{2+} influx

(Puerto et al. 2012). An extensive study by Dworkin et al. 2009 found that the downstream cAMP target, CREB, has an essential role in neurogenesis of the developing mouse brain, where it is found to be constitutively active during neural progenitor cell differentiation, and only “transiently activated outside the neurogenic regions” (Dworkin et. al. 2009).

Because axonal elongation and neuronal connectivity are so dynamic during development, it is important to consider the dysregulating influence that mutated ADCY5 might contribute during embryonic stem cell differentiation to a neuronal lineage, and specific to dopamine-containing neurons (which are involved in motor control) that are often implicated in other motor disorders such as Parkinson's disease (reviewed in Girault JA, and Greengard 2004; reviewed in Money and Stanwood 2013). ADCY5 knockout mice develop a movement disorder, displaying Parkinsonian-like movements. Interestingly, their symptoms were worsened by stress (Chen YZ 2012); and stress is a known exacerbator of patients with ADCY5-related dyskinesia (Fernandez et al. 2001; Chen DH et al 2015; Dy et al. 2016). Looking at the biochemical regulation of ADCY5, it is also known that adenylate cyclase activity is “modulated through dopamine signaling” (reviewed in Girault JA, and Greengard 2004). Dopamine receptors, with excitatory (D1) and inhibitory (D2) subclasses, are responsible for modulating the ion channel permeability upon dopamine binding, thereby influencing the neuronal membrane potential (Girault, and Greengard 2004). These changes in membrane potential may then in turn affect neuron action potentials. Abnormal firing of motor neurons has been proposed by Chen YZ et al. 2012 as a possible explanation for the myokymia seen

in such motor diseases. D1 and D2 are G-protein-coupled receptors that activate and inhibit ADCY5, respectively (Chen DH et al 2015; Puerto et al. 2012; Iwamoto et al. 2003). Both D1 and D2 are abundant in the striatal regions of the brain, regions that are responsible for movement and motor learning (Chen YZ, et al 2012; reviewed in Money and Stanwood 2013)

Of relevance, dopamine-containing neuronal innervation, as well as dopamine receptor expression is dynamic during early development and continues long after birth. It has been suggested that "This prolonged developmental timeline provides a large window of critical periods during which potential disruptors can induce varied effects" (reviewed in Money and Stanwood 2013). Because the striatum (enriched with ADCY5), receives innervation from dopamine-containing neurons, any disruptors of this pathway could be proposed as problematic. In fact, this may be responsible for the broad-spectrum of clinical presentation (Chen DH et al. 2015) that we see with ADCY5-related dyskinesia.

Research Aims

It remains unclear how mutations in ADCY5 contribute to the disease phenotypes of ADCY5-related dyskinesia at the cellular level. Evidence suggests that mutant forms of ADCY5 result in increased intracellular levels of cAMP in HEK cells. However, it is not known if the ADCY5 disease phenotypes are a result of changes in cAMP

production, or degradation, and if these changes affect development, cellular function, or both. If increased levels of cAMP in these mutations do affect neuronal differentiation, this would create changes in development and/or the connectivity of neurons and may account for the differences we see in phenotypes amongst patients with the same mutation. This study sought to address the question of whether cAMP concentration affects the differentiation of dopamine-containing neurons and if endogenous cAMP levels are affected by endogenous expression of the most common mutation seen in patients with ADCY5-associated dyskinesia, p.R418W. To address these questions, the following aims were proposed:

1. **Determine if db-cAMP levels affect differentiation of mouse embryonic stem cells into dopaminergic neurons.** It is unknown if the effects of the ADCY5 mutations on disease phenotype results from changes in development, cellular function, or both. To better explore this question, mouse embryonic stem cells were treated with a synthetic, membrane permeable form of cAMP, N6,2'-O-dibutyryladenosine 3':5'-cyclic monophosphate sodium (db-cAMP) at a range of concentrations (0, 350 μM, 700 μM, 1400 μM or 2800 μM), to see if cAMP affects differentiation to dopaminergic neurons.

2. **Creation of a CRISPR-induced ADCY5 point mutation, c.1252C>T, in HEK 293T cells.** Although overexpression of ADCY5-GFP fusion protein, containing the mutation, p.R418W, increases cAMP production in 293T cells, when pharmacologically activated using beta-adrenergic agonists (Chen YZ et al.2014), it

is not clear if cAMP production is affected when ACDY5 is pharmacologically activated in cells that express the mutation from the endogenous loci. To test this, we created the c.1252C>T (p.R418W) mutation in HEK 293T cells using the CRISPR/Cas9 genome editing system. The mutation was made by first designing the sgRNA to target the specific sequence of exon 2 in the ADCY5 gene that contains the variant nucleotide of interest. Cas9 made the cut just 5' upstream to the protospacer adjacent motif (PAM) sequence. This point mutation was repaired with the desired nucleotide (thymine) by providing the cells with a single-stranded template oligo of 150 bp long. The mutation was confirmed by PCR amplifications, followed by sequencing. The initial goal was to stimulate cAMP production in these endogenously mutated cells by pharmacological regulation with the agonist, isoproterenol, then quantify the amount of cAMP produced, using an enzyme-linked immunosorbent assay (ELISA). However, because other non-silent mutations were also created directly upstream and downstream the variant nucleotide, ELISA was not performed. Optimization of the CRISPR-induced mutation to reduce or eliminate off-target effects is pre-requisite to performing ELISA, so that in the future, these genomic editing tools would be useful to the scientists working with the patient family cell lines through our collaboration with Rare Science.

MATERIALS AND METHODS

Neuronal Differentiation of Mouse Embryonic Stem Cells

J1 murine embryonic stem cell culture

Mouse embryonic cell, J1 cell line, derived from a 129S4/SvJae male blastocyst (ATCC® Cat# SCRC1010) (American Type Culture Collection (ATCC®), Manassas, VA). mESCs were plated on a MEF layer of 30,000 cells/cm^2 of mitomycin C treated p2 mouse embryonic fibroblasts (MEFs, CytoSpring LLC, Mountain View, CA) at 30,000 cells/cm^2 in culture dishes pre-treated with 0.1% gelatin solution (STEMCELL Technologies™ Inc, Vancouver, BC, Canada or EMD Millipore, Temecula, CA). Cells were maintained at 37° C in 5% CO_2 in mESC culture media (1% of 2.0 mM L-alanyl-L-glutamine (STEMCELL Technologies™ Inc, Vancouver, BC, Canada), 1% of 1x nonessential amino acids (STEMCELL Technologies™ Inc, Vancouver, BC, Canada), 0.1% of 1000x 2-mercaptoethanol (Sigma- Aldrich®, Louis, MO), 0.1% of ESGRO® Mouse Leukemia Inhibitory Factor (LIF) (EMD Millipore, Temecula, CA), 15% of fetal bovine serum and 82.8% of DMEM (Life Technologies, Grand Island, NY and ATCC®, Manassas, VA). Approximately 72 hours post initial culturing, mESCs were passaged at 50% confluency to remaining MEF wells.

EB formation

mESCs were harvested at 50% confluency and plated on 0.1% gelatin-coated TC dishes for 48 hours. The mESCs were harvested with 0.05% trypsin EDTA and plated in suspension culture at 500,000 cells/well in a 6-well ultra-low adherent dish (Sigma-Aldrich®, Louis, MO) in 3 mls of differentiation media (15% of ES-Cult ™ fetal bovine serum (STEMCELL Technologies™ Inc,Vancouver, BC, Canada), 10 mM of MEM Non- Essential Amino acids, 2 mM of L-glutamine (Life Technologies, Grand Island, NY), 1 mM of 1-thioglycerol (Sigma- Aldrich®, Louis, MO) and DMEM media (Life Technologies Life Technologies, Grand Island, NY and American Type Culture Collection, Manassas, VA). Cells were incubated for 4 days. Media was changed every other day by transferring the media and EB's from each well to a sterile 15 ml conical tube, allowing settling to the bottom of the conical tube for 5 minutes. Spent media was removed and replenished with 3 ml of new differentiation media.

Nestin enrichment

EBs were transferred to 6-well tissue culture plates and incubated for 7 days. Cells were fed every other day with ITSFn media prepared in-lab: 1X DMEM-F12 (Gibco™ Life Technologies, Grand Island, NY), 5 µg/ml insulin (Sigma-Aldrich®, St. Louis, MO), 50 µg/ml apotransferrin (Athens Research, Athens, GA), 30 nM sodium selenite (Alfa Aesar, Haverville, MA), 250 ng/ml fibronectin (Sigma-Aldrich®, St. Louis, MO), 2.5 mM L-alanyl-L-glutamine (Gibco™ Life Technologies, Grand Island, NY).

Expansion of nestin positive cells

On day 7 of enrichment, cells were harvested, triturated into a single-cell suspension, and plated on sterile coverslips at 75,000 cells/cm^2 for all treatments and replicates. Sterile coverslips were prepared by incubating in 15 µg/ml of poly-L ornithine (Sigma- Aldrich®, Louis, MO) for 30 minutes at room temperature, rinsing 3 times in sterile PBS, followed by incubation in 1 µg/ml laminin (STEMCELL Technologies™ Inc, Vancouver, BC, Canada) for 3-5 hours at 37° C. The cells were expanded for 4 days of incubation, feeding every other day in N3 media (ITSFn media plus 20 nM progesterone, 100 nM putrescine (all from Sigma-Aldrich®, St. Louis, MO), and 1 µg/ml laminin (STEMCELL Technologies™ Inc., Vancouver, BC, Canada or EMD Millipore, Temecula, CA), 500 ng/ml Shh, 10 ng/ml bFGF, and 100 ng/ml FGF8b (all from STEMCELL Technologies™ Inc, Vancouver, BC, Canada or EMD Millipore, Temecula, CA).

Dopamine-containing neuronal differentiation

Dopaminergic differentiation was initiated by the removal of cytokine bFGF from N3 media and the addition of 200 µM ascorbic acid. Cells were fed every other day for 10 days, and pre-designated wells were treated on feeding days with 0 µM, 700 µM, 1400 µM, or 2800 µM db-cAMP, N6,2'-O-dibutyryladenosine 3':5'-cyclic monophosphate sodium (CAS# 60-92-4) (Sigma- Aldrich®, Louis, MO).

Immunocytochemistry

On the tenth day of dopaminergic differentiation, cells on coverslips were fixed with 4% paraformaldehyde in PBS for 20 minutes at 4° C. Paraformaldehyde was discarded, and cells were washed twice with PBS. The cells were then treat with 70% ETOH at room temperature for 5 minutes, rinsed once with rinsing buffer (0.25% Triton™-X-100 (Sigma- Aldrich®, Louis, MO) in PBS, and treated with blocking buffer blocking buffer (2% goat serum (Thermo Fisher Scientific, Waltham, MA) in 0.25 %Triton™-X-100 (Sigma- Aldrich®, Louis, MO) in PBS) for 30 minutes at room temperature . After blocking, cells were incubated with primary antibody, mouse- anti-beta-tubulin III (Cat # MAB1195, Lot # HGQ011611) (R&D Systems, Minneapolis, MN) for one hour at room temperature, followed by four washes with rinsing buffer for 5 minutes each. Goat anti-mouse secondary antibody-Texas Red™ (Ref # T862, Lot # 1880649) (Invitrogen™, by Thermo Fisher Scientific, Waltham, MA) was added for one

hour at room temperature in dark conditions, followed by three washes with rinsing buffer. All antibodies were diluted in working buffer (1% BSA, 0.1% Triton-X in PBS). After the secondary antibody incubation and rinses, cells were incubated in blocking buffer for 30 minutes at room temperature. Blocking buffer was removed and the additional primary antibody was added: mouse-anti-TH (Cat# AB152, Lot 2861858) (R&D Systems, Minneapolis, MN), and incubated for 1 hour at room temperature. Coverslips were then rinsed four times in rinsing buffer with 5 minutes for each wash. The additional secondary antibody was added: goat anti-mouse Alexa-Fluor™ Plus 488 (Ref# A3273, Lot # SE250296) (Invitrogen™, by Thermo Fisher Scientific, Waltham, MA) and incubated for 1 hour at room temperature, then rinsed three times with rinsing buffer, 5 minutes each wash. Stained cells were mounted on glass slides with 10 µl of ProLong® Gold antifade reagents with DAPI (Life Technologies, Grand Island, NY), and left to dry at room temperature overnight.

Images were taken using a Zeiss Axio Observer Z1 Fluorescent Microscope at 200X total magnification using 350 nm excitation and 450 nm emission filters to visualize DAPI, 595 nm excitation and 615 nm emission filters to visualize Texas Red and 490 nm excitation and 520 nm emission filter was used for the visualization of green fluorescence.

Neuronal cell quantification

ZEN 2.3 software modules for image analysis and colocalization (Carl Zeiss Inc, Thornwood, NY) were used to quantify total cell number, Tuj1 and TH positive cells. Four field of view images were taken per replicate of each treatment and the total number of cells were summated. The total numbers per replicate were then averaged to generate the average number of cells of per treatment. Both Tuj 1 and TH positive cells were then divided by the total cell population, represented by the average DAPI nuclei count. Tuj 1 and TH positive cell percentages out of total cell population were then used to perform a one-way ANOVA. In addition, TH positive cells were also divided by the number of Tuj1 positive cells to get the percent dopaminergic neuron type out of total number of neurons.

CRISPR Cas9 HEK 293T Genome Editing

HEK 293T cell culture

HEK 293T cells (Lenti-XTM) (Clontech, Mountain View, CA) were cultured in 90% Dulbecco's Modified Eagle Medium (DMEM, Life Technologies, Grand Island, NY) and 10% fetal bovine serum (Life Technologies, Grand Island, NY) and incubated at 37°C in 5% CO2. HEK 293T cells were plated in 2 ml of fresh growth media/well, at a density of 30,000 cells/cm^2. Cell number and viability were assessed using trypan blue assay, in a 1:10 dilution with a 0.4% Trypan Blue solution (Life Technologies, Grand Island, NY). Cells were counted, using 10 µl of cells in Trypan Blue, loaded on both sides of a hemocytometer, then visualized by inverted microscope, at 100X total

magnification. Cells were then passaged at 30,000 cells/cm^2. Media was replenished when the media color was orange or yellow, indicating increased acidity, from depletion of nutrients, and buildup of H protons. The cells were subcultured when they reached 90 % confluency.

ADCY5 genomic primer design

Forward and reverse primers targeting ADCY5, exon II were designed by web tool, Primer-BLAST (Ye et al. 2012. accession # NG_033882.1), to amplify a 441 bp region that includes the variant nucleotide of interest. Primers flank all of exon 2, that includes the variant nucleotide. (Figure 3). ADCY5 Primers (Integrated DNA Technologies, Skokie, IL) were tested on genomic DNA extracted from HEK 293T cells. Primer sequences are as follows:

Forward: 5- AGGACATCAGAGAGCCCGAT -3'

Reverse: 5'- GCTGGCAGCCGTAATAAGC -3.

sgRNA and repair template design

CRISPR protocol (Addgene, Cambridge, MA) (www.addgene.org/crispr/zhang) was followed for editing of the 441 bp region of interest. Both single guide RNA's (sgRNA) design were completed by entering desired sequence of exon 2 of human ADCY5 (Accession # NG_033882.1) into www.crispir.mit.edu web tool to generate guide options with various scores of off targeting effects. Higher scores are inversely proportional to off targeting effects. The chosen sgRNAs were as follows:

(5’-GGAGACCTCAGCCGGATAGT GGG-3’ with score of 93 out of 100) (“original” sgRNA); and later, for a dual nickase approach, a second sgRNA was added: 5’-CACCGCCCGAGAGTGCATCCAGGCG-3’, score of 94). The sgRNA-Cas9 vector construct was used to target the sequence in ADCY5 exon 2 that contains the variant nucleotide, as well as the 5’ protospacer adjacent motif (PAM) sequence, within the correct reading frame. A single-stranded 150 bp repair template (Integrated DNA Technologies, Skokie, IL), that spanned between the Cas9 cut site and the variant nucleotide, was created for homology directed repair, in order to obtain the missense mutation c.1257C>T, as well as a silent mutation in the PAM sequence from CCC to CAC, in order to prevent Cas9 from repetitious cutting after editing.

Px459 BpiI digest

Digestion of the initial Px459 (PsPCas9(BB)-2A-Puro (PX459) V2.0 vector, and later the PX462 (PsPCas9(BB)-2A-Puro (PX459) V2.0) vector was performed according to protocol (Addgene, Cambridge, MA) (www.addgene.org/crispr/zhang). Each digestion included 1 µg of plasmid, 1 µl Fast Digest BpiI (Cat# FD1014) (Thermo Scientific, Waltham, MA), 1µl Fast AP (Thermo Scientific, Waltham, MA), 2 µl 10X Fast Digest Buffer (Cat# EF0651) (Thermo Scientific, Waltham, MA), 14.5 µl ddH_20, and incubated for 30 min at 37°C.

Annealing and phosphorylation of forward and reverse sgRNA oligos

Addgene protocol (Addgene, Cambridge, MA) (www.addgene.org/crispr/zhang) was followed for annealing, phosphorylation and ligation of forward and reverse sgRNA oligos. 2 µl of each forward and reverse sgRNA oligo (100 µM) (Integrated DNA Technologies, Skokie, IL) was combined with 2 µl of 10X T4 Ligation Buffer (Cat# B0202S) (New England Biosciences®, Ipswich, MA), 13 µl ddH_20, and 1 µl T4 Polynucleotide kinase (Cat#M021S) (New England Biosciences®, Ipswich, MA).

Thermal cycle conditions were as follows:

37°C for 30 min,
95°C for 5 minutes
ramp down to 25°C at 5°C/min (0.08° C/sec)

Ligation

The Addgene protocol for ligation was followed (Addgene, Cambridge, MA) (www.addgene.org/crispr/zhang). After amplification, a working dilution of annealed/phosphorylated sgRNA oligos was made at 1:200 for ligation. The ligation of annealed/phosphorylated oligos to vector included: 2 µl of Bpil-digested Px459 plasmid, 1 µl annealed/phosphorylated oligos (1:200), 5µl 2x Quick Ligation Buffer™ (Cat# B2200S) (New England Biosciences®, Ipswich, MA), 3 µl dH_20, and 1 µl T7 DNA Quick Ligase™ (Cat# M0318S) (New England Biosciences®, Ipswich, MA). The ligation reaction was incubated at room temperature for 10 min.

Bacterial transformation

Transformation of the initial plasmid PX459 V2.0, and later PX462 (Addgene, Cambridge, MA) was performed by combining 2 µl ligation product (Px459 + sgRNA insert) with 50 µl Max Efficiency DH5α competent cells (Cat # 18258-012) (Invitrogen™, Thermo Fisher Scientific, Carlsbad, CA), then incubating on ice for 2 min, heat shock for 45 seconds at 42ºC, and back on ice for 1 minute. SOC media (450 µl) was added and bacteria were incubated at 37°C for 30 min, shaking at 225 rpm, before plating 100 µl onto pre-warmed LB-ampicillin (50 µg/ml)-Agar plates, then incubated at 37º C, overnight.

Colony PCR

Confirmation of proper cloning of the insert was confirmed by single colony PCR. The growth of colonies on LB-ampicillin plates indicated a likely successful bacterial transformation, as the no-transformation control plates produced no growth, and the empty-vector transformation control plate had very few colonies, due to background re-annealing of plasmid. Individual colonies were selected at random from the transformation plate with a sterile toothpick and swished in individual PCR tubes containing PCR cocktail. EconoTaq Plus® 2X PCR Master mix (reagent) and EconoTaq Plus® protocol (Cat # 30035-1) (Lucigen®, Palo Alto, CA) were used, along with previously designed sgRNA oligo (Integrated DNA Technologies®, Skokie, IL) as the forward primer and a vector-specific reverse primer (Integrated DNA Technologies®, Skokie, IL) to target the area of interest, generating an expected amplicon product of 100

bp, which included our sgRNA. Primers were diluted 1:50 and used in the PCR reaction with the following thermal cycle conditions:

95°C x 2 min, for initial denaturation
95°C x 30 sec
52.2°C x 1 min
72°C x 30 sec
Repeat 30 cycles
Final extension at 72°C x 5 min

Mini-culture, plasmid mini-prep, and glycerol stocks

Colonies that produced PCR products of correct amplicon size (100 bp) were chosen for plasmid mini-prep purification to be used in later transfection. First, those same colonies were selected again with a sterile toothpick and placed in individual tubes containing LB-broth ampicillin (50 µg/ml), and grown overnight at 37º C, shaking at 225 rpm, according to protocol (Addgene, Cambridge, MA). Approximately 14 hours later, half of the broth was used for a plasmid mini-prep, and the other half combined with equal volume of sterile glycerol and froze at -80ºC for preservation. Plasmid mini-prep purification was performed according to protocol (Ref # 740499.50) (Macherey-Nagel, Inc., Bethlehem, PA): Bacterial cell pellets were lysed and clarified before DNA was bound to spin columns, pellets were washed in buffer supplemented in ethanol, spin column membranes were dried by centrifugation, and DNA eluted in 50 µl elution buffer. Plasmid concentration was determined by NanoDrop 1000 spectrophotometer (Thermo Fisher Scientific, Waltham, MA).

Transfection of HEK 293T cells

Transient transfection of PX459-sgRNA construct into HEK 293T cells was performed using the Lipofectamine 3000® protocol (Ref L3000-008) (Life Technologies, Grand Island, NY). Experimental design included 2 replicates of transfected wells, 2 replicates of empty-vector transfected control wells, and 2 wells of non-transfected HEK cells. Cells were transfected when they reached 90% confluency with 250 ng sgRNA-Px459 construct as well as 1 µg of the 150 bp single-stranded repair template for homology directed repair. For visual confirmation of effective transfection, all cells in all

wells, except the non-transfection control wells were transfected with 750 ng of the pMAX vector containing a green fluorescent protein and a puromycin resistance gene (Cat# D-00069) (Lonza, Basel, Switzerland). GFP expression was confirmed and documented 24 hours post-transfection with a Zeiss Axio Observer Z1 Fluorescent Microscope at 200X total magnification. (Carl Zeiss Inc., Thornwood, NY).

Puromycin selection

Upon visual confirmation of transfection efficiency, cells were treated with 2.5 ug/ml puromycin added to the media to allow for sgRNA-Px459-transfected colony selection. Media was changed daily and puromycin treatment repeated every 24 hrs until all non-transfected HEK cells were dead (approximately 67 hrs). HEK cells were treated with 0.05% trypsin to harvest wells individually and transferred to 10 cm plates, plated at 5,000 cells total per plate and cultured until individual colonies were able to be visualized by microscopy.

Single Clone Selection

Upon colony formation, the individual transfected clones were passaged without trypsin. Using a P10 micropipette, under a 10X objective, individual clones were aspirated and transferred to a well of a 96-well tissue culture plate for culture. Each time cells reached 90-100% confluency, individual clones were successively passaged to 24 well tissue culture plates, then 12-well plates, and finally transferred to 6-well plates before harvesting individually for genomic DNA extraction. When harvested, half of

each clone was cryopreserved in freezing media (50% FBS, 40% DMEM, and 10% DMSO) and the other half pelleted and stored frozen at -20°C, until DNA extraction.

293T cell genomic DNA extraction

Extraction of genomic DNA from transfected HEK293T frozen cell pellets was performed according to Qiagen DNeasy blood and tissue kit and protocol (Cat # 69504) (Qiagen, Germantown, MD), and quantified by NanoDrop 1000 spectrophotometer (Thermo Fisher Scientific, Waltham, MA).

Sequence confirmation of genomic edit

Initial confirmation of CRISPR editing was performed by screening genomic DNA from sgRNA-transfected HEK clones for correct amplicon size using polymerase chain reaction (PCR). EconoTaq Plus® 2X PCR Master mix (Cat # 30035-1) (Lucigen®, Palo Alto, CA) was used, with previously designed ADCY5 primers to confirm band size, as well as single amplified product present per transfected clone. A non-transfected genomic DNA sample was used as a positive control. Clones producing a single correct amplicon product size (~440bp), were sent out for sequencing (Sequetech, Mountain View, CA). Forward and reverse genomic ADCY5 primers previously designed and confirmed to target the locus of interest were used:

Forward: 5- AGGACATCAGAGAGCCCGAT -3’

Reverse: 5’- GCTGGCAGCCGTAATAAGC -3.

Sequence chromatograms were then analyzed by Snapgene Viewer 4.2 software (Chicago, IL).

Statistical Analysis

Statistical tests were performed using R statistical software 2013. A one-way ANOVA was used to analyze all data, and Tukey's Pairwise comparison was used to determine significance between groups. The data was described as the mean +/- the SEM.

TABLES

Table 1: ADCY5 mutations associated with ADCY5-related dyskinesia, including protein domain, and case documentation (adapted from Douglas et al. 2017). Mosaic cases within families listed.

Study	New cases	# of cases genotyped, out of (total affected)	ADCY5 Mutation	Protein Domain
Chen YZ et al. 2012	1 Family	10(19)	c.2176G>A	C1b
Chen YZ et al. 2014	2 Sporadic (1 mosaic)	2	c.1252C>T	C1a
Carapito et al. 2015	1 Family	2	c.2088 + 1G>A	C1b
Menacci et al. 2015	1 Family (1 mosaic), 1 Sporadic	3	c.1252C>T	C1a

Study	New cases	# of cases genotyped, out of (total affected)	ADCY5 Mutation	Protein Domain
Chen DH et al. 2015	1 Family (1 mosaic) 8 Sporadic (3 mosaic) 3 Sporadic (1 mosaic) 1 Sporadic 1 Sporadic 1 Family (1 mosaic) 1 Family (1 mosaic)	16 3 1 1 6(12) 4	c.1252C>T c.1253G>A c.2176G>A c.3086T>A	C1a C1a C1b C2a
Chang et al. 2016	2 Families 2 Sporadic 1 Family 1 Sporadic	6 3 1	c.1252C>T c.1252C>G c.1253G>A	C1a C1a C1a
Dy et al. 2016	1 Sporadic 1 Sporadic	1 1	c.2080_2088del c.1252G>T	C1b C1a
Zech et al. 2016	1 Family 1 Sporadic 1 Sporadic 1 Sporadic 1 Sporadic	2 1 1 1 1	c.2180G>A c.1378A>T c.1196C>T c.1400A>G c.3625A>G	C1b C1a C1a C1a C2b

Study	New cases	# of cases genotyped, out of (total affected)	ADCY5 Mutation	Protein Domain
Meijer et al. 2016	1 Sporadic	1	c.1252C>T	C1a
Westenberger 2017	1 Sporadic 1 Sporadic	1 1	c.3045C>A c.3074A>T	C2a C2a
Douglas et al. 2017	1 Family	4(5)	c.3086T>G	C2a

Table 2: Display of DAPI count averages per replicate and overall average, and std. dev. and std. error within each treatment. Three replicates of each were listed for each treatment level, except for 2800 µM, which included two replicates, due to loss of third.

Replicate	No treatment	700 µM	1400 µM	2800 µM
1	3603	2352	6689	6649
2	4026	5122	6368	6504
3	2939	4758	6756	
Average	**3522.66**	**4077.33**	**6604.33**	**6576.50**
Std dev	**547.93**	**1505.22**	**207.39**	**102.53**
Std error	**316.35**	**869.04**	**119.73**	**72.50**

Table 3: Statistics for average percent Tuj1 neurons/total cell population (DAPI). Std. dev and Std. error of percent Tuj1 positive cells within each treatment displayed.

Treatment (TX)	Ave # Tuj1	Ave # DAPI	Tuj1 ÷ DAPI X 100%	Standard Deviation	Standard Error
No Tx	398	3,524.33	11.38 %	4.60	1.32
700 µM	499.66	4077.33	14.02 %	6.64	1.91
1400 µM	622.33	6604.33	9.80 %	3.06	0.88
2800 µM	468	6576.50	7.45 %	3.30	1.16

Formatted Table

Table 4: One-way ANOVA statistical output. Statistical output of one-way ANOVA of percent Tuj1 neurons/total cell population (DAPI), gives a P-value (<0.05), indicating there is a *significant difference in mean percent Tuj1 positive cells amongst treatment levels.

	DF	Sum Sq	Mean Sq.	F-Value	P-Value
Treatment	3	228.9	76.31	3.393	0.027*

Table 5: Tukey's pairwise comparison for 95% confidence interval for percent Tuj1 neurons/total cell population (DAPI) , displays the 700 µM treatment-2800 µM pair are the most significantly different: adjusted p-value (0.02) indicates a significant difference between the mean of 700 µM and 2800 µM treatment levels.

Pair	diff	lwr	upr	P.adj
700-2800 µM	6.5661	0.7641	12.3680	0.0211*
Residuals	40	899.6	22.48	

Table 6: db-cAMP treatment does not affect percent TH positive cells out of total cell population (DAPI). The average TH positive cells divided by total cell population (DAPI). Std. dev, and Std. error within each treatment level displayed.

Treatment	Ave # TH	Ave # DAPI	TH ÷DAPI x 100%	Standard Deviation	Standard Error
No TX	124	3,524.33	3.51 %	1.76854961	0.510536297
700 µM	191	4077.3333	5.43 %	3.520809237	1.01637008
1400 µM	228.33333	6604.3333	3.58 %	1.399712453	0.404062181
2800 µM	181	6576.5	2.89 %	1.190447928	0.420886901

Table 7: One-way ANOVA statistical output. P-value for percent TH positive cells out of total cell population (DAPI) is not significant (>0.05).

	DF	Sum Sq.	Mean Sq.	F-value	P-value
Treatment	3	39.43	13.142	2.599	0.0655
Residuals	40	202.23	5.056		

Table 8: db-cAMP treatment does not affect percent TH positive cells out of total number of neurons (Tuj1). TH positive cells/Tuj1 positive cells. Std. error within treatment levels calculated.

	No Tx	700 µM	1400 µM	2800 µM
% TH	31.15 ± 0.02	38.22±0.04	36.68±0.01	38.9±0.01

Table 9: One-way ANOVA statistical output. P-value not significant (>0.05).

	Df	Sum	Mean sq	F-value	P-value
Treatment	3	374.3	124.78	2.109	0.114
Residuals	40	2367.0	59.17		

Table 10: Summary of CRISPR-induced point mutation attempts. Each CRISPR attempt listed, including what sgRNA and vector used, and edits made to PAM sequence, and variant nucleotide.

Attempt	sgRNA	Vector	Correct PAM edit made?	Variant nucleotide edited?	Off target effects?
1	original	Px459	No. 2/3 had different edit made.	No.3/3 sequences with ambiguous base-calling, with one detectable wild-type	Ambiguous base calling after Cas9 cut site.
2	original	Px459	Yes. 6 /10	10/10 wild-type	Minimal ambiguous base-calling.
3	Original + Second Dual Nickase	Px462 X 2	1/6	5/6 wild-type 1 G>T edit on reverse strand	Point mutations and large INDELS
4	original	Px459	No	2/37 with correct edit, some wild-type, and other edit types	Point mutations

Table 11: Fold-change values (normalized to GAPDH by densitometry) of TH and D2R in 1400 µM cAMP-treated neurons comparing to neurons with no cAMP.

Sample Name	Fold-change to no treatment
Cytosolic TH	**1.15**
Membrane TH	**-2.51**
Cytosolic D2	**1.73**
Membrane D2	**2.06**

FIGURES

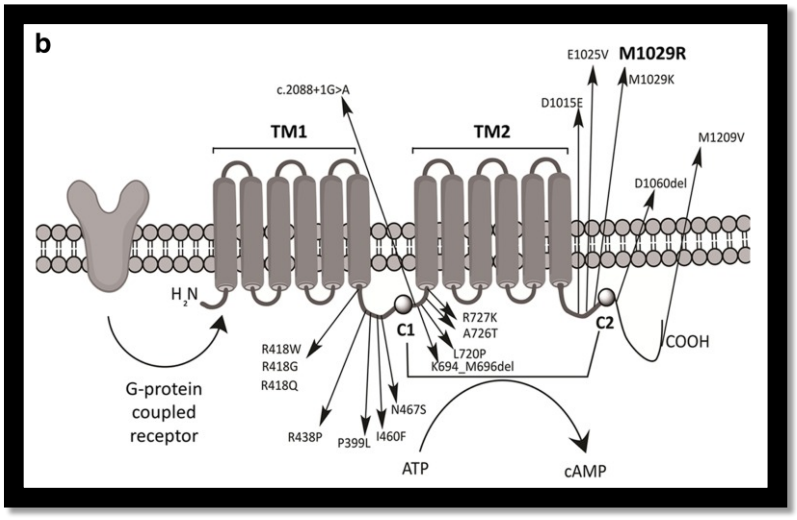

Figure 1: Schematic of the protein structure adenylate cyclase transmembrane proteins. The mutations identified in individuals with ADCY5 are annotated. Note all mutations are located in catalytic domains C1 and C2. (Douglas et al. 2017).

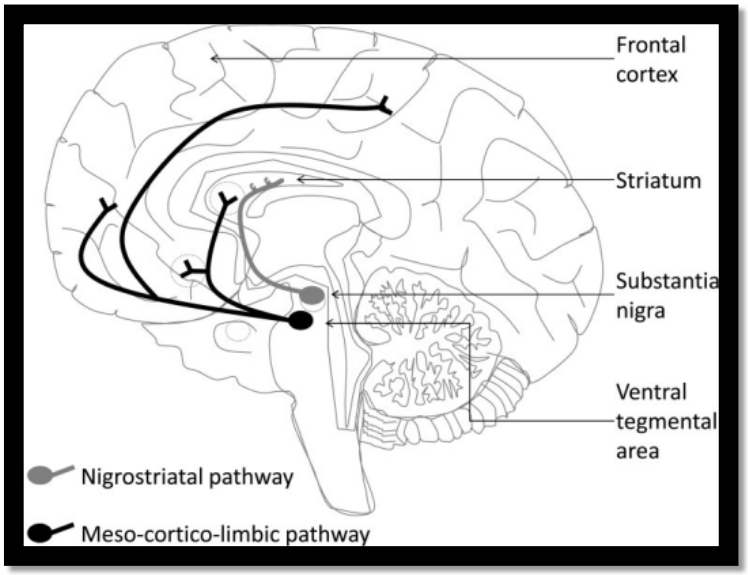

Figure 2: Schematic drawing of a midsagittal cross section of the human brain. Display of the medial location of the striatum, and the nigrostriatal pathway (dopaminergic motor pathway), in relation to the meso-cortico-limbic pathway (Brunelin et al. 2013). From the schematic, we see the dopaminergic motor pathway projects from the substantia nigra, up to the striatum.

```
100741 gacatatccc atgacaagcc agccaaactt ctggctttga ggacatcaga gagcccgatc
100801 gattatgctc ggctgctcac agtggttggc cgcgtgtggg gtgccctcag catttgtttg
100861 ctagcgccag gtgtgagttt gctgagacag gggctgaggg cttcatgctt tggggccagg
100921 aaggtcagga tctgagctag gtgtgctcct ctctccctct gcagcttgtc tccaatgttc
100981 tcattttctc ctgcaccaac atcgtgggtg tctgcaccca ctatccggct gaggtctccc
101041 agagacaggc tttccaggag acccgagagt gcatccaggc gcggctccac tcgcagcggg
101101 agaaccagca gcaggtgagt gaggcccctg cccttgcaca gtgggacgga gtcgagccct
101161 gagatgtacc tcagctgagt gcctggccta gggcgggcag tgcttattac ggctgccagc
101221 cccactcccc gggaggggac caacccatgg ggaatgtttc ccctggagag agtccagcat
```

Figure 3: The entire exon 2 sequence of human ADCY5 (NG_033882.1). The intron (not highlighted) and exon (grey-highlighted) genomic sequences are displayed. The forward genomic primer is underlined, and reverse genomic primer is in bold print; primers were used to target the genomic region that contains the variant.

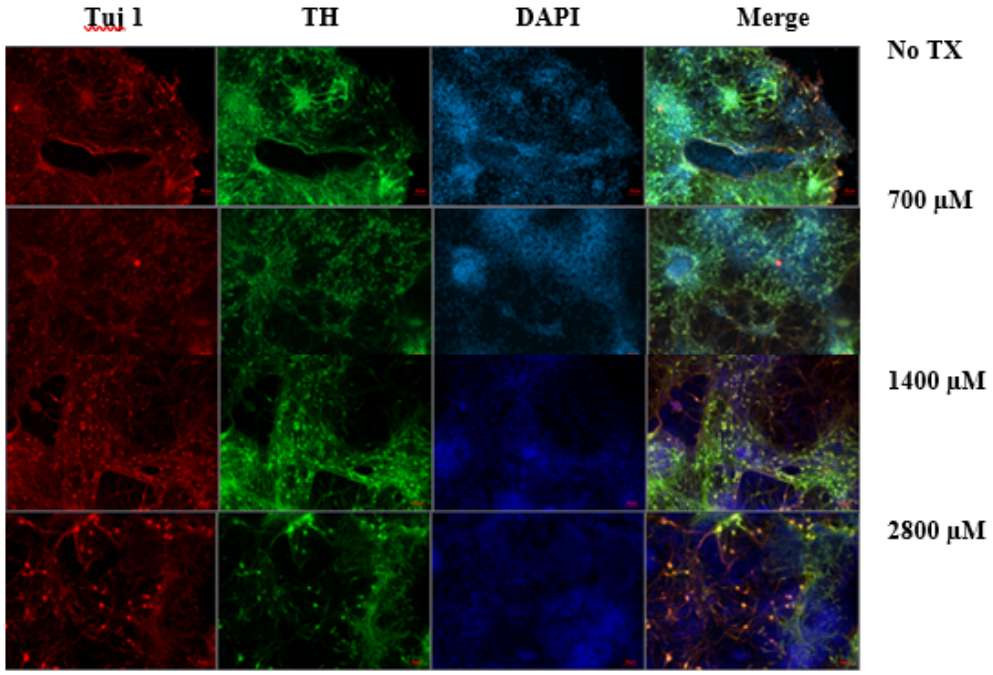

Figure 4: db-cAMP treatment affects dopaminergic differentiation of murine embryonic stem cells. ICC images of neurons day 10 of differentiation, displayed per treatment, taken at 200X total magnification. Tuj1: a class III beta tubulin neuronal cell marker. Tyrosine Hydroxylase (TH): dopaminergic cell marker. DAPI: nuclei staining. Merge images visually demonstrate an increase in neurons with 700 µM treatment, and then a decrease in overall neuron count with the higher db-cAMP treatments.

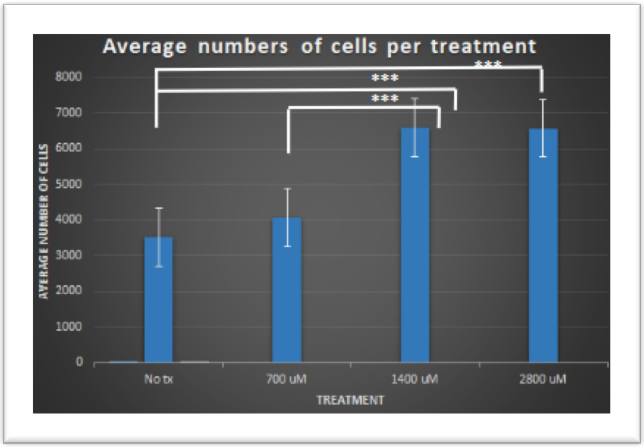

Figure 5: db-cAMP treatment affects the average number of DAPI. Error bars display mean +/- SEM. Average number of DAPI stained nuclei/treatment level was generated by the summation of DAPI count within four field of views, and then averaged by the three replicates/treatment level. This process was repeated for Tuj1 and TH. The bar graph displays an increasing trend in overall cell count for DAPI stained nuclei. One-way ANOVA was significant (P-value=7.05 $x10^{-08}$ ***).

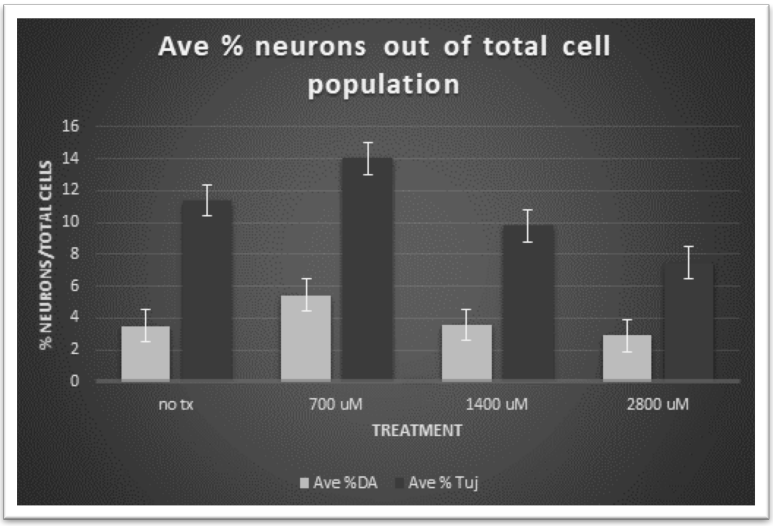

Figure 6: db-cAMP treatment affects percentage of Tuj 1 and TH out of total cell population (DAPI). Bar graph of percent average neurons, represented by Tuj1 positive cells, divided by the total cell population (DAPI) per treatment. Side by side comparison with percent average TH positive cells divided by the total cell population (DAPI), per treatment. Percent Tuj1 and TH cells display similar trend of dramatic increase with 700 µM treatment, and then a continual decrease with the higher cAMP treatment. Error bars display mean +/- SEM.

A).

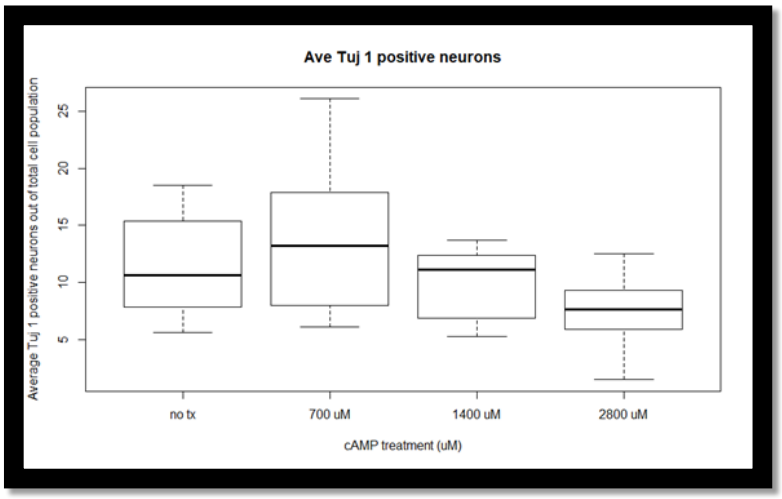
Ave Tuj 1 positive neurons
Average Tuj 1 positive neurons out of total cell population
5
10
15
20
25
no tx
700 uM
1400 uM
2800 uM
cAMP treatment (uM)

B).

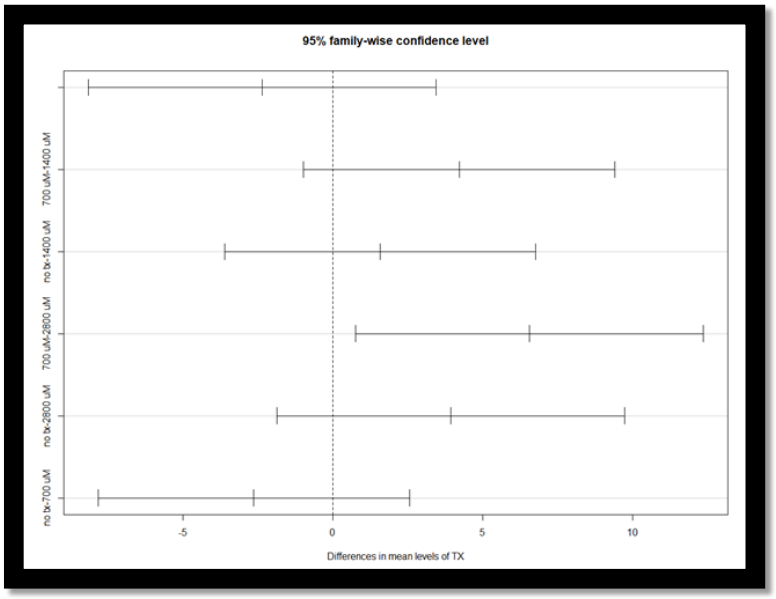

Figure 7: One-Way ANOVA statistical output displays db-cAMP treatment has a significant effect on percent Tuj1 positive neurons out of the total cell population. A). Box plots display the interquartile range of percent Tuj1 positive neurons amongst treatment levels, with the median for each treatment level indicated by the black bar. **B).** Tukey's pairwise comparison graph for 95% confidence interval, displaying the 700 μM treatment-2800 μM pair are the most significantly different, as the only pair whose confidence interval does not include zero.

A).

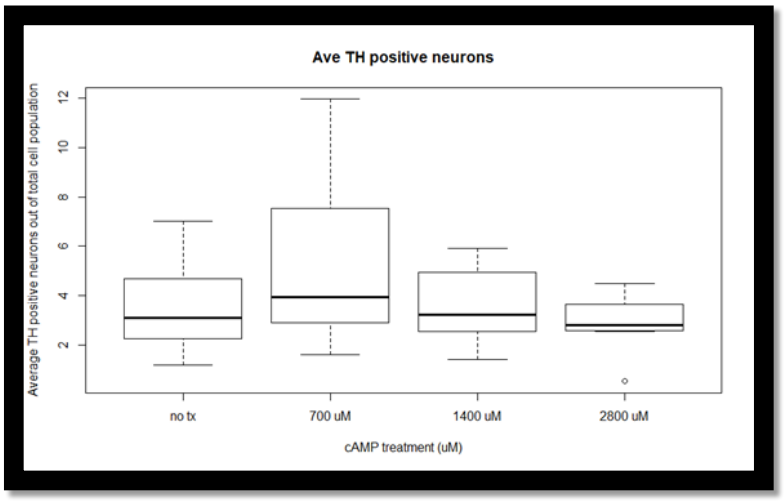
Ave TH positive neurons
Average TH positive neurons out of total cell population
2
4
6
8
10
12
no tx
700 uM
1400 uM
2800 uM
cAMP treatment (uM)

B).

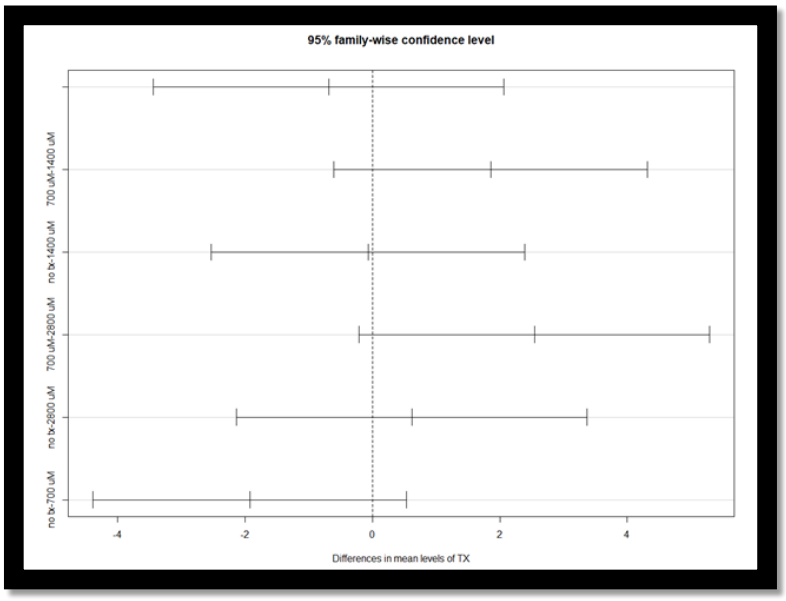

Figure 8: The one-way ANOVA displays db-cAMP treatment does not affect percent TH positive neurons out of the total cell population (DAPI. TH positive cells divided by the total cell count (DAPI). **A).** Box plots display the interquartile range of percent TH positive neurons amongst treatment levels, with the median for each treatment level indicated by the black bar. **B).** Table of TH/DAPI calculations and statistical output of one-way ANOVA, gives a P-value (0.06), indicating there is a borderline significant difference in mean percent TH positive cells amongst treatment levels. **C).** Tukey's pairwise comparison graph for 95% confidence interval, displaying the 700 µM treatment-2800 µM pair are the most different, however not considered statistically significant.

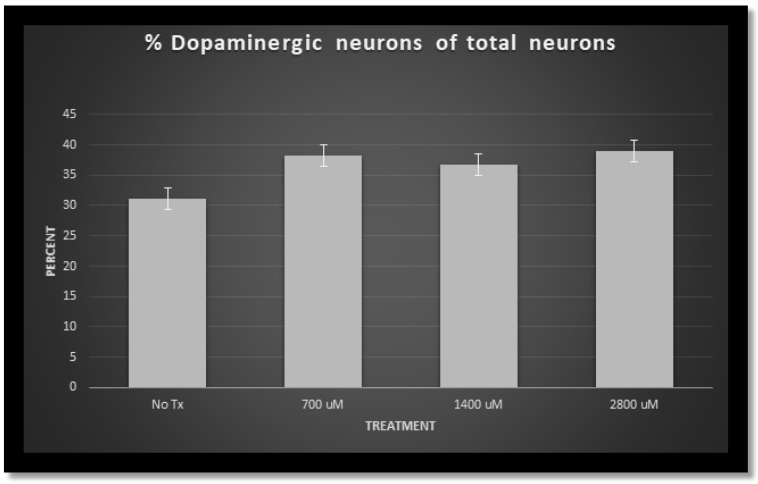

Figure 9: db-cAMP treatment does not significantly affect the percent TH positive cells out of total number of neurons (Tuj1 positive cells). Error bars display mean +/- SEM. TH positive cells divided by total number of neurons (Tuj1), displays a slight increase in percent TH with 700 μM treatment, then a slight decrease with 1400 μM treatment, followed by a slight increase with 2800 μM treatment.

A).

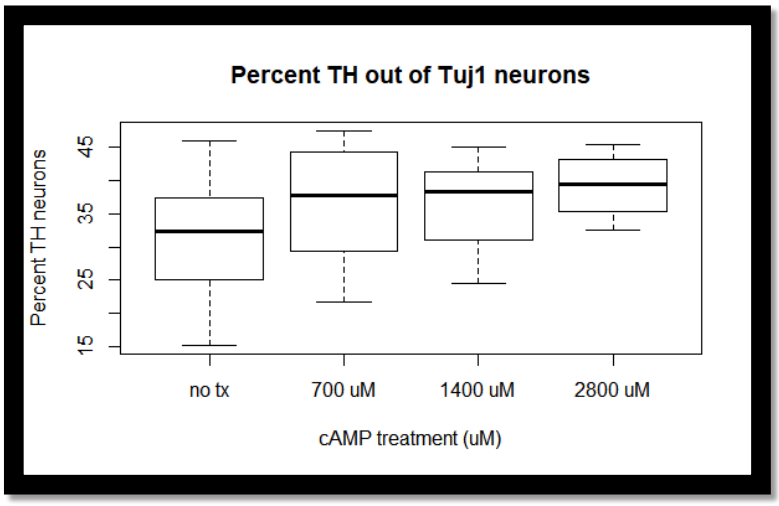
Percent TH out of Tuj1 neurons
Percent TH neurons
15
25
35
45
no tx
700 uM
1400 uM
2800 uM
cAMP treatment (uM)

B).

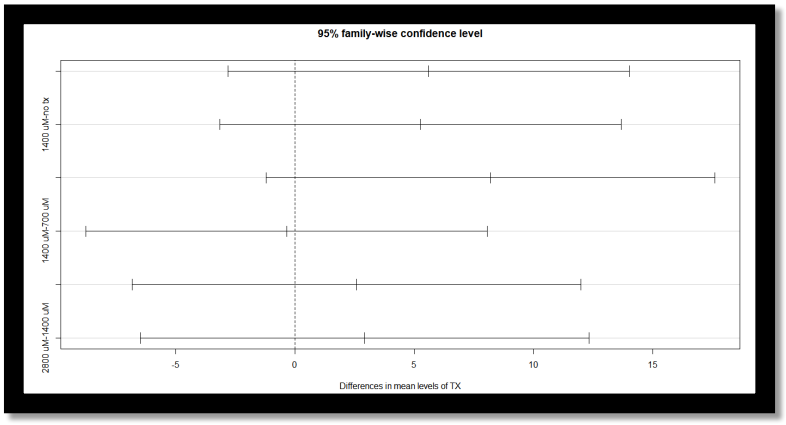

Figure 10: The one-way ANOVA displays db-cAMP treatment does not affect percent TH out of total neurons (Tuj1). **A**. Box plot of percent TH/Tuj1 displays the interquartile range of percent TH positive neurons amongst treatment levels, with the median for each treatment level indicated by the black bar. **B.** Tukey's pairwise comparison graph for 95% confidence interval, displaying the no treatment-2800 μM pair are the most different, however not considered statistically significant.

A).

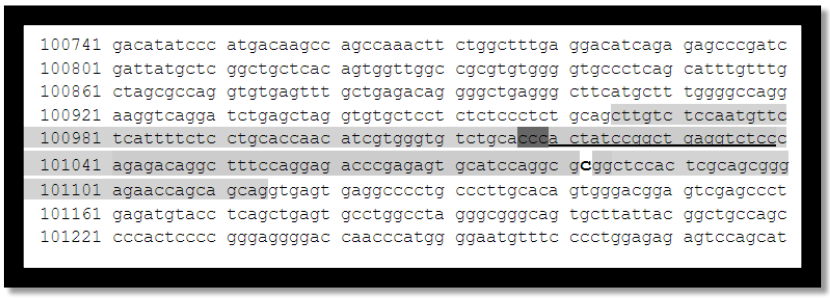
100741 gacatatccc atgacaagcc agccaaactt ctggctttga ggacatcaga gagcccgatc
100801 gattatgctc ggctgctcac agtggttggc cgcgtgtggg gtgccctcag catttgtttg
100861 ctagcgccag gtgtgagttt gctgagacag gggctgaggg cttcatgctt tggggccagg
100921 aaggtcagga tctgagctag gtgtgctcct ctctccctct gcagcttgtc tccaatgttc
100981 tcattttctc ctgcaccaac atcgtgggtg tctgcaccca ctatccggct gaggtctccc
101041 agagacaggc tttccaggag acccgagagt gcatccaggc gcggctccac tcgcagcggg
101101 agaaccagca gcaggtgagt gaggcccctg cccttgcaca gtgggacgga gtcgagccct
101161 gagatgtacc tcagctgagt gcctggccta gggcgggcag tgcttattac ggctgccagc
101221 cccactcccc gggaggggac caacccatgg ggaatgtttc ccctggagag agtccagcat

B).

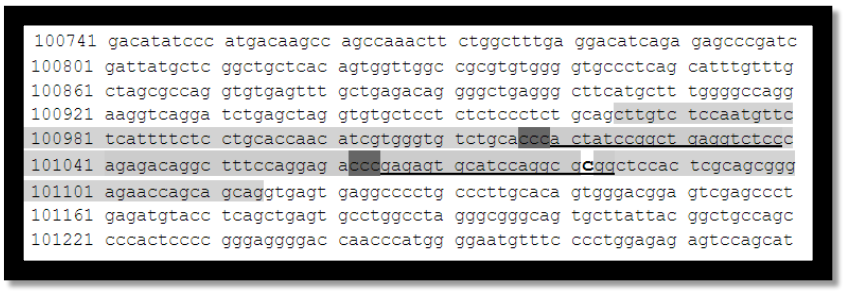
100741 gacatatccc atgacaagcc agccaaactt ctggctttga ggacatcaga gagcccgatc
100801 gattatgctc ggctgctcac agtggttggc cgcgtgtggg gtgccctcag catttgtttg
100861 ctagcgccag gtgtgagttt gctgagacag gggctgaggg cttcatgctt tggggccagg
100921 aaggtcagga tctgagctag gtgtgctcct ctctccctct gcagcttgtc tccaatgttc
100981 tcattttctc ctgcaccaac atcgtgggtg tctgcaccca ctatccggct gaggtctccc
101041 agagacaggc tttccaggag acccgagagt gcatccaggc gcggctccac tcgcagcggg
101101 agaaccagca gcaggtgagt gaggcccctg cccttgcaca gtgggacgga gtcgagccct
101161 gagatgtacc tcagctgagt gcctggccta gggcgggcag tgcttattac ggctgccagc
101221 cccactcccc gggaggggac caacccatgg ggaatgtttc ccctggagag agtccagcat

C).

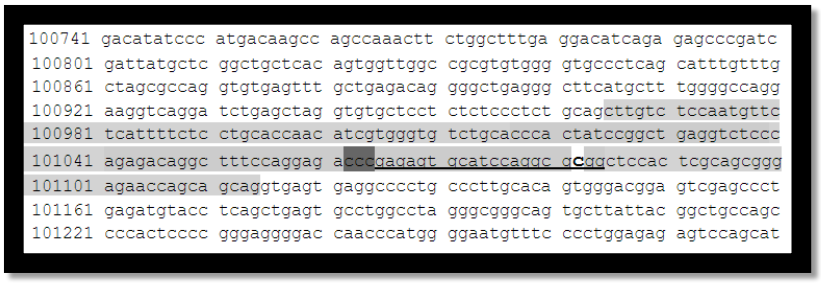

Figure 11: sgRNA design to target region of variant nucleotide, for CRISPR-induced c.1252C>T mutation. The entire exon 2 sequence of human ADCY5 (NG_033882.1) (shaded in light grey) within its genomic DNA region (non-shaded)**. A). CRISPR attempt #1 and 2:** PAM (shaded dark grey), targeted sgRNA sequence (underlined), and variant nucleotide (capitalized and bolded). Cas9 will cut just 5' to the PAM sequence (CCC). **B). CRISPR attempt # 3:** dual nickase approach, including both original (underlined), and the second sgRNA (underlined) to target variant nucleotide (capitalized and bolded). Both PAM sequences highlighted in dark grey. **C). CRISPR attempt # 4:** Used only the second sgRNA (underlined), which targets a PAM sequence (dark grey highlighted) closer to variant nucleotide (capitalized and bolded).

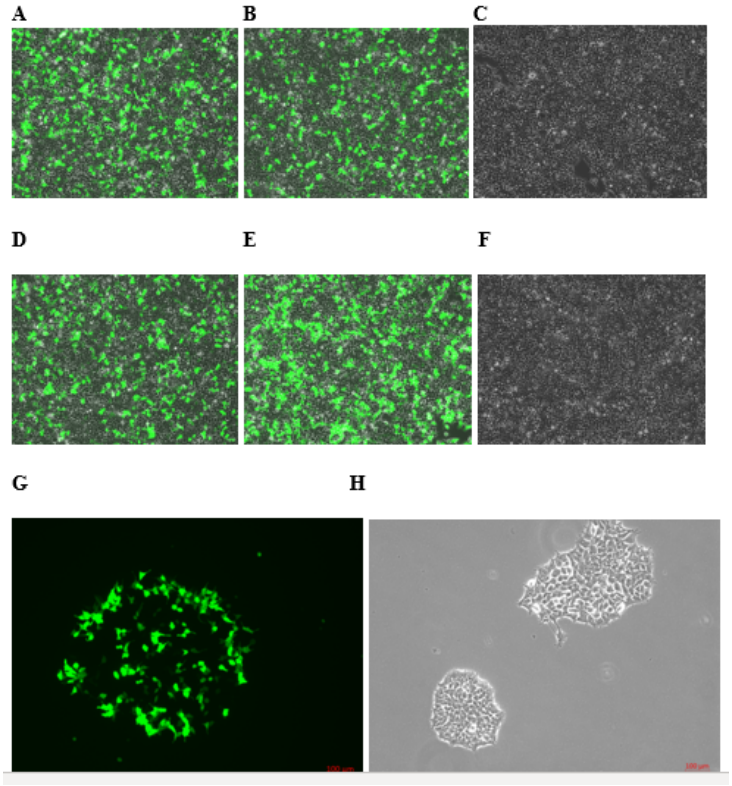

Figure 12: Successful transfection of sgRNA and GFP into HEK 293T cells, 24 hours post-transfection (CRISPR attempt # 4). A and **B**. replicates of sgRNA/GFP transfected 293T cells, displaying GFP expression, indicating good transfection efficiency. **C**. non-transfected control displays absence of GFP expression, as expected. **D** and **E.** empty-vector transfection controls, GFP expression indicates good transfection efficiency. **F.** Non-transfected control replicate displays absence of GFP as expected. **G.** Fluorescent image of a sgRNA and GFP-transfected HEK clone (200X total magnification). **H.** Brightfield image of sgRNA and GFP-transfected HEK clones (200X total magnification).

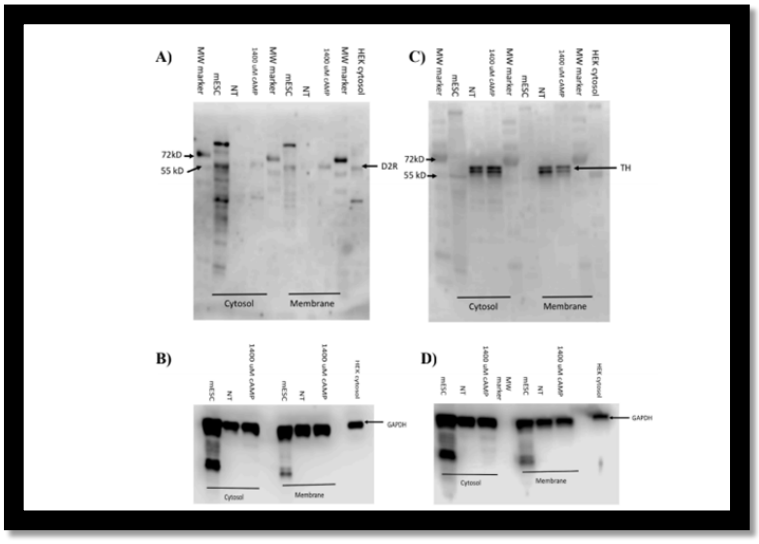

Figure 13: Treatment with db-cAMP increases D2R's expression in cytosol and membrane of 1400 µM-treated neurons; cAMP affects TH's expression in the cytosol and membrane of 1400 µM-treated neurons. A). 1400 µM cAMP treated neurons express approximately 2-fold more D2R in the cytosol and membrane compared to neurons with no treatment (NT). mESC is negative control; HEK 293T is positive control. Each lane has 10 µg of protein. **B).** GAPDH blot for normalizing to D2R. **C).** cAMP treated neurons express approximately 1.15-fold more TH in the cytosol and 2.51-fold less in the membrane compared to neurons with NT. mESCs and HEK 293T are negative control. **D).** GAPDH blot was used for normalizing to TH.

RESULTS

cAMP Treatment Affects Neuronal Differentiation of Mouse Embryonic Stem Cells

Aim I: determine if cAMP levels affect differentiation of murine embryonic stem cells into dopamine-containing neurons.

My first aim was designed to determine if cAMP levels affect differentiation of mouse embryonic stem cells into dopaminergic neurons. My hypothesis was that increased cAMP during neuronal differentiation would have some effect on either total cell numbers, number of neuronal cell type, morphology of neurons, or all of the above. We optimized the dopamine-containing neuronal differentiation protocol published by Kwon et al. 2014, to achieve efficient directed differentiation of mESCs into dopamine-containing neurons, confirmed by the presence of Tuj1 and TH, using immunocytochemistry (ICC)

cAMP treatment affects morphology of neurons

The ICC results demonstrate neuron morphological change with increasing cAMP treatment (Figure 4). Looking across the treatments, we see a high concentration of bundle of neuronal processes, which appears to be slightly increased with the 700 μM treatment. The 1400 μM treatment produces a decrease in the number of neurons present,

as well as a change from bundles of neuronal processes, to semi-sparse collection of neurons, with more prominent somata. We see a dramatic change in morphology in the 2800 μM treated cells, specifically the least dense presentation of neurons, and most prominent somata.

cAMP treatment affects the overall cell population

Through quantification software post ICC, we were able to confirm cell count differences amongst db-cAMP treatments and perform statistical analysis on those results. The number of cells counted/treatment based on DAPI, display an increasing trend from no treatment to 1400 μM db-cAMP, average cell counts increase, followed by a decrease in average cells counts with the 2800 μM treatment (Figure 5) (Table 2).

cAMP treatment affects the percent of Tuj1 positive cells in the population

The effect of db-cAMP on the percent of Tuj1 positive cells (representing putative neurons) out of the total cell population also seems to change with dosage of db-cAMP. Visualized by ICC, the density of neurons appears to increase with 700 μM treatment compared to no treatment. There is a marked continual decrease in neuron density from 700 μM to 1400 μM and 2800 μM. This threshold effect suggests that at higher cAMP treatment, there is a decrease in the overall percentage of cells that differentiate into neurons. Cell quantification, followed by statistical analysis of the percentage of Tuj1 cells, confirm this interpretation. Box plots display a dramatic increase in the percent of Tuj1 positive cells from no treatment to 700 μM db-cAMP, then it tapers back down in

the 1400 μM treatment and even lower in 2800 μM treatment. (Figure 6) (Table 3). For the percentage of neurons (Tuj1 positive cells) out of the total numbers of cells (DAPI count), the one-way ANOVA (Table 4) showed there was a significant difference in the mean percent amongst treatments (P-value<0.05); specifically, the Tukey's pairwise comparison (Table 5) shows that the mean percent of Tuj1 positive cells in the 700 μM treatment is significantly different from the 2800 μM treatment (adjusted P-value=0.021) (Figure 4). Although visually and quantitatively we see an increase in percent Tuj1 with the 700 μM treatment vs. no treatment, this is not significantly different from the no treatment.

db-cAMP treatment does not affect percent TH positive cells out of total cell population (DAPI)

For the percent of TH positive cells (representing dopamine-containing neurons) out of the total cell population (DAPI count), we see a similar trend as with percent Tuj1/DAPI; there is a dramatic increase in the mean percent of TH positive cells from no treatment to 700 μM, then it tapers down in the 1400 μM and 2800 μM (Table 7). Because Tuj1/DAPI and TH/DAPI display similar trends, we suspected that cAMP might not affect TH positive cells specifically, but overall neuronal differentiation efficiency. To confirm this, the percentage of TH positive cells out of the Tuj1 positive cells were determined, and results are discussed under the next heading. A one-way ANOVA was performed (Table 7) on percentage of TH-expressing cells out of the total number of cells, as indicated by DAPI staining. The ANOVA was not significant (P-value=0.065)

db-cAMP treatment does not affect the percent of TH positive cells out of total neuronal cell type

The percent of Tuj1 cells that are *also* TH positive represent those neurons who have differentiated to produce dopamine (Table 8). The one-way ANOVA for TH/Tuj1 reveals there is not a significant difference amongst mean percent TH out of total neurons (Tuj1) (Table 9).

The Creation of the ADCY5 p.R418W Point Mutation in 293T HEK Cells.

Aim II: characterize the effect of p.R418W mutation on cAMP levels in HEK cells

My second aim sought to characterize the effect of the p.R418W mutation on cAMP levels in 293T HEK cells. Our hypothesis, based on previous research by Chen et. al. 2014, predicted that this point mutation produces higher levels of cAMP in mutant cells, compared to wild-type, when stimulated with the agonists, forskolin and isoproterenol. To attempt to characterize endogenous expression levels of cAMP in cells with the p.R418W mutation, a CRISPR sgRNA-plasmid construct was designed to transfect 293T cells and target the ADCY5 gene, exon II, to create a double stranded break just 5' to the PAM sequence, upstream the variant nucleotide c.1252 (Figure 11). A repair template with the desired mutation was provided during transfection, to use the

cell's own homology directed repair mechanism to edit the variant nucleotide to the desired mutation: c.1252 C>T CRISPR genome editing of HEK 293T cells was attempted a total number of 4 times, each with a slight modification of the previous attempt (Table 7).

Confirming Transfection Efficiency

To confirm transfection efficiency of our sgRNA-plasmid construct in all attempts, a GFP-plasmid was also transfected simultaneously, then visualized by fluorescent microscopy. Each CRISPR attempt produced an average transfection efficiency of over ~80 percent. In the final attempt, the presence of green fluorescence in transfected cells about an 80-90 percent transfection efficiency (Figure 12).

Confirmation of CRISPR Edit

The creation of CRISPR-induced c.1252C>T point mutation in 293T cells was attempted a total of four times in order to achieve the correct edit (Table 10). Our first attempt we used the aforementioned sgRNA and PX459 vector, however, due to technical difficulties, single colony selection did not produce many viable transfected clones and

few that survived did not contain the edit upon sequencing. All sequences revealed ambiguous base-calling, after PAM cut site. One of those clones revealed wild-type at variant nucleotide. Two out of three sequences revealed an incorrect PAM edit: CCC to CGC, and the other CCC to GCC (Appendix A).

The second attempt did not include any changes to the sgRNA; however, technique optimization of the single colony selection improved survival of clones. More clones (32 experimental, and 5 control clones) were harvested and, based on PCR clone selection, ten experimental and one control were sequenced. Sequence results of experimental clones revealed all sequences were wild-type (Appendix B). However, some of the clones contained the silent PAM mutation. The 5' end of sequences were fairly clean, until downstream the Cas9 cut site, where some sequences revealed ambiguous base calling, indicating the target site was cut, but repair introduced INDELS and other mutations. The control clone revealed wild-type at variant nucleotide and the PAM sequence, as expected.

Because sgRNA-dual-nickase approach has been shown to be more efficient at on-target CRISPR genome editing than sgRNA (Gopalappa et al. 2018), the third CRISPR attempt included the use of the original sgRNA, and a second sgRNA ("dual nickase") targeting nearer to the variant nucleotide. Both original and dual nickase sgRNA were cloned into a new vector (PX462) that contained D10A Cas9 mutation, allowing for a single stranded cut from each sgRNA-Cas9 construct. Single colony selection was again successful, with 53 experimental clones, and 12 control clones. After initial screening by PCR for confirmation of a single amplicon of correct size, six

experimental clones and one control clone were sequenced. Sequence results revealed all clones remained wild-type at the variant nucleotide, except for one clone (#10) that contained the desired edit on the reverse strand (Appendix C). All sequences contained ambiguous base calling between the 5' PAM and the variant nucleotide. It is also likely that a mixed population of transfected HEK cells was obtained during initial single colony selection, as this is an inefficient process even though optimization of technique improved harvest. The purified PCR product of clone # 10 was later subcloned to determine if there were mixed alleles. Sequence results of subcloning revealed sequences from a mixed cell population due to more than two alleles. (Appendix D). Only one of the six experimental clone sequences contained the correct "CCC" to "CAC" PAM edit, the rest did not (Appendix E). The control clone sequence revealed a clean (non-ambiguous base calling) sequence with wild-type variant nucleotide and no PAM edit, as expected (Appendix F). BLAST analysis on the control sequence revealed 99% homology to wild-type human ADCY5 exon II.

The fourth and final CRISPR attempt was optimized based on the observation of previous attempt #2, where the PAM edit was made with minimal to no off-targeting effects, even though the variant nucleotide was not editing. It seemed likely that the clean PAM edit was due to the cut site's proximity to the repair site, in this case the PAM repair was made because the cut site was only two nucleotides upstream. Therefore, for the last CRISPR attempt, the second sgRNA that we designed for dual nickase was cloned into the original vector (PX459), allowing for a double stranded break in closer proximity to the variant nucleotide. This second sgRNA-Cas9 made the cut 20 bp

upstream this time, as opposed to 65 bp upstream as in our second attempt. Single colony selection was the most efficient this fourth attempt, with the initial selection of 300 clones. A total of 43 clones (39 experimental and 4 control) were used to harvest genomic DNA. PCR screening was performed on all 39 experimental clones, and 4 control clones (two from each replicate of the initial empty-vector transfection controls, and one non-transfected control). PCR results revealed a high success of single PCR product of correct size (Appendix G). Of the 39 experimental clones, 37 were sequenced, along with control clones, and one non-transfected control. Sequence chromatograms revealed various edits of the variant nucleotide, with some clone sequences that contained a c.1252C>G edit, as well as other mutations, there were some that remained wild-type, and some had too many ambiguous base-calls to read the sequence accurately (Appendix H). Successfully, there were two sequences (#13 and #36) that contained the correct c.1252C>T edit in the forward strand (Appendix I). However, these two sequences also contained other non-silent mutations directly upstream and downstream the variant nucleotide. None contained the PAM edit, as expected because the new cut site is just 5' to the new PAM sequence, which is downstream the original PAM sequence (Appendix J). All control clones contained wild-type sequences as expected. BLAST analysis of control clones showed 99 percent identical to wild-type (Appendix K).

DISCUSSION

Dopamine-Containing Differentiation

I have demonstrated through directed differentiation of mouse embryonic stem cells that db-cAMP treatment *in vitro* does in fact affect total cell numbers as well as percentage of cells that undergo neuronal differentiation. Based on the average DAPI count, our experiments reveal an overall increasing trend of total cell population starting from no treatment up 1400 µM and 2800 µM treatment. This suggests that increased cAMP during differentiation affects either non-neuronal cell differentiation or survival, yet without the dramatic drop in cell count at higher the cAMP treatments, as we see with neuronal cell type. This difference in the trend of cell count between non-neuronal and neuronal cell types indicates increased cAMP influences general cell numbers, but its distinct effect is also cell-type specific.

Amongst treatment levels of db-cAMP, we also observed an effect on the neuronal morphology and number, represented by Tuj1 positive cells, out of the total cell population (DAPI count). As reported in the results, ICC visually reveals that with increasing db-cAMP concentrations, there is a continual change in neuronal arrangement. There seems to be a threshold for producing changes in neuronal presentation, with a dense presentation of bundles of neuronal processes in the no treatment and 700 µM, to a striking decrease in neuronal density with the higher cAMP treatments (indicated by a loss of TH or Tuj 1 signal). We even see a continual change from 1400 µM to 2800 µM,

where not only are neurons the sparsest, but visually, the fluorescent signal of the somata become more prominent. This visual pattern we see is reflected in the quantification of neurons (Tuj1 positive cells) out of total cell population amongst treatments; there is an initial increase in percent Tuj1 positive cells with 700 µM treatment, then a tapering down at the higher cAMP levels. The biological interpretation of the effect that higher cAMP has on the neuronal cell population is that during early development, a gain-of-function mutation in ADCY5 is likely to affect the initial production of neurons, long before it may influence differentiation of these neurons to specific neuronal cell type, such as dopaminergic.

Examining the effects of db-cAMP treatment on dopamine-containing differentiation, represented by TH positive cells, out of the total cell population (DAPI count), we see the same visual pattern on ICC as we do with the Tuj1 cells. The no treatment controls display bright, clustered TH positive neurons, with a subtle increase in TH signal in the 700 µM merge image, then we start to lose TH signal in the 1400 µM, and then only a small amount of distinct TH signal present with 2800 µM, where projections are sparse. Quantitative analysis of TH count divided by DAPI count, yielding percent TH positive cells, confirms ICC results, and mimics the percent Tuj1 positive cells' pattern: a slight increase in percent with the 700 µM treatment, and then tapers down in 1400 µM and continued in 2800 µM db-cAMP.

Because the percent TH positive cells out of DAPI count results followed the pattern of results obtained for percent Tuj 1 out of DAPI, we suspected that the increase in percent TH population seen at 700 µM may just be due to the increase in overall

neuron count (Tuj1). We addressed this by dividing TH cells by Tuj1 cells, which removed DAPI background and allowed for TH to Tuj1 ratio. As reported in the results section, the percent TH out of total neuron population (Tuj1) was negligible and not statistically significant. Therefore, we concluded that cAMP does not affect the percent dopamine-containing differentiation efficiency, but rather affects neuronal differentiation. This information ties back to what was stated earlier in this discussion, that higher levels cAMP during early development could affect neuronal cell type, prior to neuron-specific differentiation. Specifically, the process of neurogenesis starts with exuberant neural progenitor cell production (NPC), followed by migration, differentiation, synaptogenesis, selective apoptosis, myelination for select neurons, and finally synaptic pruning. However, many neurons remain non-myelinated. (reviewed in Kristiansen M, and Ham J**.** 2014).

Other studies that have included cAMP treatment during cell culture include research by Branton et al. 1998, where they demonstrated that treatment with db-cAMP, ranging from 500 µM to 1000 µM of a cell suspension made from rat embryonic ventral mesencephalon, , showed a dramatic increase of TH positive cell survival at the 700 µM level, and then a gradual decrease above 700 µM concentration. This coincides with the threshold effect we see in our experiments with cAMP treatment, from an increase in neuronal production at lower concentrations, to a decrease in higher levels. However, that study did not include a general neuronal cell marker such as Tuj1. It is likely that the pattern that they are describing could be due to an overall increase in general neuron population, as we determined in our study. In a different study by Rolletschek et al. 2001,

they report the addition of survival promoting factors that included 700 µM db-cAMP, during in vitro differentiation of mESCs to dopaminergic neurons, produced an increase in the percentage of cells, expressing TH mRNA, with an upregulation from 9 percent (on day 4) to 76 percent (on day 16). Also, in a genome-wide profiling study of dopaminergic differentiation of hESC (Momĉilović et al. 2014), cAMP synthesis was identified as one of the upregulated pathways, and they demonstrated that the addition of 200 µM db-cAMP during in vitro dopaminergic differentiation increased DA neuron yield by 5 %. In an earlier study by Michel and Agid, 1996, found that the addition of db-cAMP specifically promotes dopaminergic development, but not GABAergic, or serotonergic neurons.

As previously described, the study by Chen et. al 2014 showed that exogenous overexpression of ADCY5 p.R418W mutation increased cAMP production, above wild-type levels, in pharmacologically activated 293T cells, using beta-adrenergic agonists, forskolin and isoproterenol. In fact, they demonstrated an almost 10-fold increase in cAMP production, compared no treatment cells, as measured by ELISA. Combining this key information with our results that demonstrate cAMP treatment affects the overall production of neurons and altered neuronal morphology, with the knowledge that ADCY5 is expression in the striatum increases dramatically during early development (Menacci et al. 2015), it is not surprising that neurogenesis during early development could be dramatically altered at any of those stages. It is likely that the decreased neuronal cell production and changes in morphology would ultimately affect

synaptogenesis, where initial cell density is crucial in determining selective apoptosis (Kristiansen and Ham 2014).

Based on the above information, one could predict that a higher level of cAMP during early development could result in the ADCY5 disease phenotype. However, it is not known what the actual cAMP concentrations are in ADCY5-related dyskinesia patients, or if there are varying cAMP concentrations amongst patients, but this could account for the wide spectrum of clinical presentations.

Other possible effects of increased cAMP levels by mutated ADCY5 may include disruption of the other components of dopamine signaling, specifically dopamine receptor expression and enzymes responsible for dopamine synthesis. Data derived from experiments conducted by Linh Pham (unpublished data 2018) seem to support this hypothesis. Linh looked at the effect 1400 μM db-cAMP on the protein expression of dopaminergic receptor (D2R) and tyrosine hydroxylase (Figure 13) (Table 11). Immunoblot analysis revealed an approximately 2-fold increase of D2R in the cytosol as well as in the membrane of the neurons differentiated in the presence of 1400 μM db-cAMP. It has been reported that "D1 and D2 receptors express distinct patterns of affinity to dopamine and interact differently with one another depending on synaptic concentrations of neurotransmitter" (reviewed in Korchounov et al. 2010). In fact, "while both D1 and D2 receptors are abundant in the striatum, the expression pattern of D1 and D2 receptors in the axon terminals, dendrites, and spines are obviously diff erent by electron microscopic analysis" (reviewed in Hisahara and Shimohama 2011). Because the D2 subtype, including D3 and D4, are coupled to inhibitory G-proteins that inhibit cAMP

production, this provides a theoretical basis to suspect that an increase in D2 postsynaptic expression would disrupt the cAMP downstream substrates such as DARPP-32, that modulate other neurotransmitters (reviewed in Hisahara and Shimohama 2011).

Looking at TH protein expression levels, there was 1.15-fold increase in cytosolic TH expression and a 2.5-fold reduction in membrane TH expression in neurons differentiated in the presence of 1400 μM db-cAMP when compared to no treatment. As a control, the results also reveal no TH expression present in mESCs or HEK 293T cells, which supports that TH expression is associated with dopamine-containing neuronal differentiation. The change in TH expression coincides with our finding that 1400 μM db-cAMP treatment causes an overall decrease in the neuronal cell population. With fewer neurons present, it is not surprising that the immunoblot analysis displayed less TH protein in the membrane fraction due to fewer available neurons, not necessarily less TH production per neuron.

Of relevance to this data interpretation is the biochemical regulation of dopaminergic signaling. Dopamine neurotransmitter is packaged in vesicles at the presynaptic axon terminal, and upon calcium influx, are released into the synaptic cleft. Excess dopamine is recycled back to the presynaptic terminal (reviewed in Daubner et al. 2011).

Tyrosine hydroxylase is the rate-limiting enzyme in the conversion of tyrosine to L-DOPA. Looking at cellular localization of TH expression in vivo, studies have shown that TH is primarily expressed in the soma cytosol, but also in the membranes of the axons and dendrites, differing in its subcellular distribution (reviewed in Pickel et al.

1975). Within the soma, TH is expressed in the membranes of the Golgi apparatus, the endoplasmic reticulum, and is soluble throughout the cytoplasm, but not found in the mitochondrial or lysosomal membranes. Within the processes, TH staining revealed organized, linear aggregates that were parallel along the length of the plasma membrane (reviewed in Pickel et al. 1975).

The enzymatic activity of tyrosine hydroxylase is inhibited by a dopamine feedback loop. TH is phospho-activated by PKA (directly downstream cAMP), and in turn, this phosphorylation makes TH less susceptible to the feedback inhibition loop. Studies also revealed that TH is associated with regulatory proteins, such as PP2A and AADC, forming complexes that aid TH proximity to secretory vesicles, allowing for quick availability of dopamine transport to vesicles (reviewed in Daubner et al. 2011).

The upregulation of the inhibitory D2 receptor coupled with the 2.5-fold decrease of TH in the membrane fraction of neurons differentiated in the presence of db-cAMP (which includes the endomembrane compartments necessary for dopamine secretion), suggests dopamine signaling is compromised in neurons exposed to high levels of cAMP. Though there was no significant change of TH expression in the cytosol (1.15-fold), this doesn't necessarily mean this population of enzymes would not be impacted by increases in endogenous cAMP, as inhibition of enzymatic activity would not be detected by immunoblot. To explore this as a mechanism related to ADCY5-dyskinesia, we would have to repeat these experiments and perform TH enzymatic assays with protein extracts from both wild type and ADCY5 mutant cells.

These data suggest that an increase in cAMP may not just affect number of neurons produced during early development, which not only would affect connectivity, but also the amount of available D2R receptors in the cytosol and membrane. The change in availability of dopamine receptors, will inevitably affect ion channel permeability upon dopamine binding, ultimately affecting neuron firing (Girault JA, and Greengard P. 2004). The work conducted by Linh Pham (2018) contributes to this project; however, it is important to take into the consideration the limitations of those experiments. The protocol used to extract membrane proteins, may not have been specific to cell membrane fraction, but might also include intracellular organelle membranes. If experiments were repeated, it would be important to use a cell membrane specific extraction protocol as well as include a cell surface specific marker in immunoblot analysis, and even an endomembrane marker to ensure we are not getting significant amounts of organelle membrane. Examining the D1 subclass receptor protein expression under cAMP conditions would also be beneficial because of its role in increasing membrane potential.

If increased cAMP during early development affects dopamine inhibitory receptor protein expression, then a plausible treatment may include D2 receptor antagonists to inhibit overproduction, or D1 receptor agonists as a compensatory treatment option; however, this option is limited because cells will often adjust receptor expression in response to exogenous drug treatment. In fact, DA excitatory receptor agonists may be an optimal choice because “DA receptor agonists exert their pharmacologic eff ect by directly activating DA receptors, bypassing the presynaptic synthesis of DA” (reviewed in Hisahara and Shimohama 2011).

When considering treatment for ADCY5 patients, it is important to note that two other movement disorders that result from disrupted dopaminergic signaling, Parkinson's (PD) and Huntington's (HT) diseases differ in their presentation compared to ADCY5-related dyskinesia (AD) patients. Both PD and HT have a much later onset in adulthood than AD patients, which can present with symptoms as early as six months of age (Menacci et al. 2015). AD patients do not usually experience cognitive defects, as is common with both PD and HT. PD is more associated with bradykinesia and akinesia and can display dementia as the disease progresses. Although HT and AD both experience dystonia, chorea, and dysarthria, AD patients are mostly affected by involuntary movements, whereas HT patients also experience impaired voluntary movement (Chen et al. 2015; Mayo Clinic 2018). It has also been reported that a unique symptom of AD is myokymia (Menacci et al. 2015), whereas a unique feature of PD is tremor (reviewed in Hisahara S, and Himohama 2011). Looking at the cellular level, another key difference is that PD has been characterized as a *loss* of kinesis function due to *loss* of midbrain dopaminergic neurons (reviewed in Hisahara S, and Himohama 2011). Only about 15 percent of PD patients have been linked to genetic mutations in LRRK2, PARK7, PINK1, PRKN, or SNCA, as well as other genes not listed here, but most cases are sporadic (NCBI 2012). HT is caused by an autosomal dominant genetic mutation in the HTT gene that causes *loss* of striatal neurons (Mayo Clinic 2018). Knowing how AD's clinical presentation is distinguished from other movement disorders and combining this knowledge with our investigation of this disease at the

cellular/molecular level, unique treatment options and timing of treatment can be customized, maximizing patient care.

The findings of this research allow for collaborators to make informed decisions about therapeutic options, specifically narrowing the selection of pharmacologic treatments, such as an ADCY5 isoform-specific inhibitor (Chen YZ et al. 2014; reviewed in Hurley 1999), or cAMP-specific PDE 4, 7, or 8 agonist (reviewed in Raker 2016) to increase degradation of cAMP. These drug treatments can be tested first on patient iPSCs for efficiency of elimination of excess cAMP, before going to clinical trials, minimizing the unnecessary trial and error on actual patients. These patient iPSCs will be critical in narrowing the gap between benchtop to bedside treatment. Individual patient genomic DNA can be used to perform exome sequencing to determine mutation-type, followed by creation of patient iPSCs, which will allow scientists to perform experiments tailored to individual patients, testing highly selected pharmacologics to determine efficacy and appropriate dosage.

CRISPR-Induced Point Mutation

Our first attempt failed due to inefficient single clone selection, and sequence results revealed that our sample was most likely from a mixed population of cells, as opposed to monoclonal. In our second attempt, single clone selection was much more efficient due to technique optimization, however sequence results all wild-type at variant nucleotide, and some correct editing of the PAM sequence. There were also other

mutations and INDELS created. In the third attempt, a dual nickase approach was used in hopes to increase efficient repair sequence results revealed mostly wild-type, with other mutations, including INDELS.

By learning from previous attempts, we optimized the final attempt by designing a sgRNA that would target closer to the variant nucleotide, in hopes to increase repair efficiency We successfully edited the variant nucleotide of interest in two transfected HEK clones out of 37 experimental clones sequenced; we were unsuccessful in making that our *only* edit. In fact, every sequence examined contained non-silent mutations. This is not surprising as CRISPR is known for high targeting efficiency but inefficient repair (reviewed in Paix et al. 2017; Aird, et al. 2018). In fact, single nucleotide edits have a low efficiency of 0.1 percent 5 percent (Komor, et al 2016). In all four attempts, we demonstrated that our sgRNA design found its target site and a cut was made, but with low repair efficiency. The fourth attempt was by far the most successful, however still needs more optimization to limit off-target mutations. This optimization can be accomplished by understanding the full capabilities of CRISPR technology and learning from what other scientists have done to optimize their CRISPR experiments.

CRISPR made its formal debut in 2012 (Jinek et al. 2012), and since then its use and breadth of application has accelerated dramatically in the field of research (reviewed in Hsu et al. 2014). Some of the initial obstacles with CRISPR included inefficient delivery by plasmid or viral vectors, which in turn can lead to overexpression of the vector, producing off-targeting editing (reviewed in Jacobi A 2017). CRISPR initially was limited to the subtype II Cas9 endonucleases, but recent developments have provided

a wider array of Cas9 endonucleases from subtypes I and II, and now with genetically engineered Cas nucleases, researchers can use enzymatically inactivated, or "dead" Cas9 (dCas9), fused with a transcriptional activator or inhibitor to allow for binding of Cas9-sgRNA complex, without cutting. The tethered dCas9 can therefore be used for gene activation or inhibition, or even epigenetic applications (reviewed in Hsu et al. 2014).

A common limitation to CRISPR editing is low efficiency of homology directed repair (Aird, et al. 2018). Because the enzymatic activity of CRISPR endonucleases can stimulate the host cell's NHEJ as well as HDR, this increases likelihood of getting nucleotide insertions and deletions, known as INDELS (reviewed in Hsu et al. 2014). From my own observations using CRISPR, it also seems likely to get off target editing, including INDELS and point mutations, based on how close the edit site is to the cut site. As seen in our initial attempts, the further downstream the edit site is to the initial cut site, the more likely of getting other editing events such as point mutations and INDELS. Our final CRISPR experimental design included a cut site that had greater proximity to the repair site, much closer than previous sgRNA-transfection attempts. This indeed improved our editing efficiency, as it was the only time we achieved the correct edit of the variant nucleotide, but still it created other off target, non-silent mutations. It is also probably that once edited, using the repair template, there are still mutations naturally occurring within the HEK 293T genome, not induced by the sgRNA transfection. Other researchers using CRISPR have circumvented the low repair efficiency by optimizing CRISPR design as well, using novel techniques. A recent study by Aird, et al. 2018 used covalent tethering of the single-stranded DNA repair template directly to the Cas9-

sgRNA ribonucleoprotein complex (non-vector delivery), to ensure presence of repair template in proximity to cut site. As reviewed in other literature, this approach has been shown to decrease the risk of an immune response from the host cell, increases the stability of the Cas nuclease, and limits the Cas9 components: allowing quick termination of cutting once the edit has been made. This thereby limits the off-targeting effects compared to vector delivery (reviewed in Jacobi A 2017). Referencing back to the Aird, et al 2018 study, their results demonstrated increased efficiency in different target loci of multiple cell types, with a 5 to 11-fold increase in HDR efficiency. They also confirmed efficiency at the gene expression level, using qPCR, and found a 2-fold increase in HDR efficiency using the tethered repair oligo method, compared to untethered Cas9.

Another approach that may improve precise editing is base editing, a modified CRISPR technique to create a point mutation within the genome without creating a double-stranded break, and conversion is deemed irreversible. (Komor et al. 2016). Base editing makes use of dCas9, fused to a cytidine deaminase enzyme, allowing for direct conversion of cytidine to uridine (essentially a C to T, or G to A transition mutations). This conversion can take place within five nucleotides of target binding. Research at the University of Harvard, Liu lab, has successfully demonstrated this base editing using four human and murine cell lines, with "permanent correction of approximately 15 percent to 75 percent of total cellular DNA with minimal (typically ≤1 percent) INDEL formation" (Komor et al. 2016).

Moving forward with the CRISPR portion of this project, future work could include: 1). A ribonucleoprotein sgRNA-Cas9 delivery. 2). Design of allele specific

primers for initial PCR confirmation of edit, for more specificity. 3). A base editing approach could be tried as an alternative to traditional CRISPR. Once a monoclonal cell line with the desired edit has been created, it would critical to then perform and optimize ELISA to quantify cAMP levels produced under mutant conditions compared to wild-type. Repeating this experiment in multiple cell lines would also be beneficial. This data could then be compared to not only the gain-of-function experiments first conducted by Chen et al. 2014, but also to compare with the levels of cAMP that produced changes in our neuronal differentiation experiment. If these cAMP levels were found comparable to the changes we saw in our neuronal differentiation experiments, this would support the hypothesis that the p.R418W mutation is likely a gain-of-function mutation, and a more definitive biological conclusion could be made about the effects of increased cAMP on cellular function and early development.

CONCLUSIONS

The data analyzed from our neuronal differentiation experiments provide a base model for understanding the pathophysiological mechanisms underlying the ADCY5-related dyskinesia phenotype. We demonstrated that cAMP levels above 700 μM do not significantly affect dopamine-containing neuronal specific differentiation, however it does significantly decrease overall neuronal cell type production, as well as change neuronal morphology. Our data supports a model where the molecular basis of ADCY5-related dyskinesia precipitates its effects during early development by altering the morphological structure of neuron fascicles and decreasing overall neuron production, before differentiation of those neurons take place, and thereby ultimately affecting neuronal connectivity and proper signaling. Based on Linh Pham's data, we also propose that downstream effects of high levels of cAMP include increased D2 protein expression levels, and decreased levels of the dopamine-synthesizing enzyme, tyrosine hydroxylase, within the membrane of neuronal processes, ultimately disrupting the balance of the striatonigral dopamine pathway.

Building upon our model, further investigation will require looking at other downstream effects of high levels of cAMP, such as excitatory D1 subtype receptors, regulation of CREB, and neurotrophic factors, NGF, PACAP, BDNF, and DARRP-32. Our findings are significant when we consider the spatiotemporal gradient of neuronal development, and ADCY5 expression. Because the striatonigral dopaminergic pathway travels through to the striatum and activates ADCY5 all through early development and

long after birth into adulthood, the expansive time frame for deleterious effects of mutated ADCY5, enriched in the striatum, provides probable cause for the broad spectrum of clinical presentation of ADCY5-related dyskinesia.

Unfortunately we are not able to compare the levels of db-cAMP that affect neuronal differentiation to levels of endogenous cAMP in cells containing the p.R418W mutation. Although not completed according to our initial aims, the CRISPR portion of this research will still provide a starting point for future optimization of a CRISPR-based assay that will be useful to our collaborators in understanding the cellular effects of not only the p.R418W mutation; it will also allow for a directed plan for analysis of the other 17 point mutations known to date. The results of these assays, specifically the quantified cAMP under each mutation type, can then be used as a baseline to compare to ADCY5-related dyskinesia patient samples. Patient samples will allow for their iPSCs to be used to perform ELISA to quantify individual levels of cAMP, comparing them to non-affected individuals as well as other patients with the same mutation, and patients with other ADCY5 mutations, ultimately expanding the database of knowledge about the molecular basis of ADCY5-related dyskinesia so treatment can be improved.

REFERENCES

Aird EJ, Lovendahl KN, St. Martin A, Harris RS, Gordon WR. 2018. Increasing Cas9-mediated homology directed repair efficiency through covalent tethering of DNA repair template. Communications Biology. 1:54. doi: 10.1038/s42003-018-00542.

Atwood BK, Lopez J, Wager-Miller J, Mackie K, and Straiker A. 2011. Expression of G protein-coupled receptors and related proteins in HEK293, AtT20, BV2, and N1 8 cell lines as revealed by microarray analysis. BMC Genomics. 12:14.

Bauer P, Kreuz FR, Bürk K, Saft C, Andrich J, Heilemann H, Riess O, Schöls L. 2006. Mutations in TITF1 are not relevant to sporadic and familial chorea of unknown cause. Mov. Disord. 21:1734–1737.

Breedveld GJ, van Dongen JWF, Danesino C, Guala A, Percy AK, Dure LS, Harper P, Lazarou LP, van der Linde H, Joosse M, et al. 2002. Mutations in TITF-1 are associated with benign hereditary chorea. Hum. Mol. Genet. 11:971–979.

Brunelin J, Fecteau S, Suaud-Chagny MF. 2013. Abnormal striatal dopamine transmission in Schizophrenia. Curr Med Chem. 20 397-404.

California Institute for Regenerative Medicine (CIRM) [Internet]. [Cited 2017 Feb 11]. Available from: https://www.cirm.ca.gov/

Carecchio M, Mencacci NE, Iodice A, Pons R, Panteghini C, Zorzi G, Zibordi F, Bonakis A, Dinopoulos A, Jankovic J, Stefanis L, et al. 2017. ADCY5-related movement disorders: frequency, disease course and phenotypic variability in cohort of paediatric patients. Parkinsonism Relat Disord. 41: 37-43.

Chang FCF, Westenberger A, Dale RC, Smith M, Pall HS, Perez-Dueas B, Grattan-Smith P, Ouvrier RA, Mahant N, Hanna BC, et al. 2016. Phenotypic insights into ADCY5-associated disease. Mov. Disord. 31:1033–1040.

Chen D, Friedman JR, Bonkowski ES, Stessman HA, Doummar D, Bernes S, Davis MY, Damon-perrière N, Swanson PD, Tranchant C, et al. 2015. Broader spectrum and genotype – phenotype correlations. Neurology. 85: 2026-2035.

Chen Y-Z, Matsushita M, Robertson P, Rieder M, Girirarja S, MBBS, Antonacci F, Lipe H, Eichler E, Nickerson D, et al. 2012. Autosomal dominant familial dyskinesia and facial myokymia: Single exome sequencing identifies a mutation in adenylyl cyclase 5. Arch. Neurol. 69:630–635.

Chen Y-Z, Friedman JR, Chen D-H, Chan GC-K, Bloss CS, Hisama FM, Topol SE, Carson AR, Pham PH, Bonkowski ES, et al. 2014. Gain-of-function ADCY5 mutations in familial dyskinesia with facial myokymia. Ann. Neurol. 75:542–549.

Daubner SC, Lee T, Wang S. 2011. Tyrosine hydroxylase and regulation of dopamine synthesis. Arch. Biochem. Biophys. 501(8): 1-12.

Dessauer C, Watts v, Rennolds O, Conti M, Dove S, Seifert R. 2017. International union of basic and clinical pharmacology structures and small molecule modulators of mammalian adenylyl cyclases. Pharmacological Reviews. 69(2): 93-139.

Do T, Sun Q, Beuve A, Kuzhikandathil EV. 2007. Extracellular cAMP inhibits D1 dopamine receptor expression in CAD catecholaminergic cells via A2a adenosine receptors. J. Neurochem.101: 619-631.

Douglas A.G.L., Andreoletti G, Talbot K, Hammans S.R., Sigh J., Whitney A, Ennis S, Foulds N.C. 2017. ADCY5-related dyskinesia presenting as familial myoclonus-dystonia. Neurogenetics. 18: 111-117.

Duman RS, and Nestler EJ. Functional Roles for cAMP and cGMP. In: Siegel GJ, Agranoff BW, Albers RW, et al., editors. Basic Neurochemistry: Molecular, Cellular and Medical Aspects. 6th edition. Philadelphia: Lippincott-Raven; 1999. Available from: https://www.ncbi.nlm.nih.gov/books/NBK27915/

Dworkin S, Malaterre J, Hollande F, Darcy PK, Ramsay R, Mantamadiotis T. 2009. cAMP Response Element Binding Protein is Required for Mouse Neural Progenitor Cell Survival and Expansion. Stem Cells. 27: 1347-1357.

Dy ME, Chang FCF, Jesus SD, Anselm I, Mahant N, Zeilman P, Rodan LH, Foote KD, Tan W-H, Eskandar E, et al. 2016. Treatment of ADCY5-associated dystonia, chorea, and hyperkinetic disorders with deep brain stimulation: a multicenter case series. J. Child Neurol. 31:1027–1035.

Fernandez M, Raskind W, Wolff J, Matsushita M, Yuen E, Graf W, Lipe H, Bird T. 2001. Familial dyskinesia and facial myokymia (FDFM): A novel movement disorder. Ann. Neurol. 49:486–492.

Girault J-A, and Greengard P. 2004. The neurobiology of dopamine signaling. Arch Neuro. 61: 641-644.

Gopalappa R, Suresh B, Ramakrishna S, Kim H. 2018. Paired D10A nickases are sometimes more efficient than individual nucleases for gene disruption. Nucleic Acids Research. 46:12: e71. Available from: https://doi.org/10.1093/nar/gky222

Hisahara S, Shimohama S. 2011. Dopamine receptors and Parkinson's disease. Int. J. of Medicinal Chem. 2011: 1-16.

Hsu PD, Lander E, Zhang F. 2014. Development and applications of CRISPR-Cas9 genome engineering. Cell. 157(6):1262-1278.

Hurley J. 1999. Structure, mechanism, and regulation of mammalian adenylyl cyclase. J. Biol. Chem. 274:7599-7602.

Iwamoto T, Okumura S, Iwatsubo K. 2003. Motor dysfunction in type 5 adenylate cyclase-null mice. J. Biol. Chem. 278:16936-16940.

Jacobi A, Rettig G, Turk R, Collingwood MA, Zeiner SA, Quadros RM, Harms DW, Bonthuis PJ, Gregg C, Ohtsuka M, et al. 2017. Simplified CRISPR tools for efficient genome editing and streamlined protocols for their delivery into mammalian cells and mouse zygotes. Methods. 121-122: 16-28.

Jinek M, Chylinski K, Fonara I, Hauer M, Doudna JA, Charpentier E. 2012. A programmable dual-RNA-guided DNA endonuclease in adaptive bacterial immunity. Science. 337: 816-821.

Katsushika S, Kawabe J-I, Homcy CJ, Ishikawa Y. 1992. In Vivo generation of adenylate cyclase isoform with a half molecule motif. J. of Biological Chem. 268: 2273-2276.

Kim K-S, Lee K-W, Lee K-W, IM J-Y, Yoo J-y, Kim S-W, Lee J-K, Nester E.J, Han L. 2006. Adenylyl cyclase type 5 (AC5) is an essential mediator of morphine action. PNAS. 103:3908-3913.

Knab AM, Lightfoot JT. 2010. Does the difference between physically active and couch potato lie in the dopamine system? Int. J. Biol. Sci. 6:133–150.

Komor AC, Kim YB, Packer MS, Zuris JA, Liu DR. 2016. Programmable editing of a target base in genomic DNA without double-stranded DNA cleavage. Nature. 533: 420-424.

Korchounov A, Meyer MF, Krasnianski M. 2010. Postsynaptic nigrostriatal dopamine receptors and their role in movement regulation. J. Neural. Transm. 117: 1359-1369.

Kristiansen M, and Ham J. 2014. Programmed cell death during neural development: the sympathetic neuron model. Cell death and differentiation. 21: 1025-1035.

Kwon Y-W, Chung, Y-J, Kim J, Lee H-J, Park J, Roh T-Y, Cho H-J, Yoon C-H, Koo B-K, Kim H-S. 2014. Comparative study of efficacy of dopaminergic neuron differentiation between embryonic stem cell and protein-based induced pluripotent stem cell. Plos One 9(1): doi.org/10.1371/journal.pone.0085736.

Ludwig and Seuwen. 2002. Characterization of the human adenylyl cyclase gene family: cDNA, gene structure, and tissue distribution of the nine isoforms. J. Recept Signal Transduct Res 22:79-110.

Matsuoka I, Suzuki Y, Defer N, Nakanishi H, Hanoune J. 1997. Differential expression of type I, II, and V adenylyl cyclase gene in the postnatal developing brain. J Neurochem. 68: 498-506.

Mayo Clinic [Internet]. [cited 2018 May 16]. Available from: www.mayoclinic.org/diseases-conditions/huntingtons-disease/symptoms-causes/syc-20356117

Mencacci NE, Erro R, Wiethoff S, Hersheson J, Ryten M, Balint B, Ganos C, Stamelou M, Quinn N, Houlden H, et al. 2015. ADCY5 mutations are another cause of benign hereditary chorea. Neurology 85:80–88.

Michel PP, and Agid Y. 1996. Chronic activation of the cyclic AMP signaling pathways promotes development and long-term survival of mesencephalic dopaminergic neurons. J Neurochem. 67:1633-1642.

Momčilović O, Liu Q, Swistowski A, Rissp-Tait T, Zhao Y, Rao MS, Zeng X. 2014. Genome wide profiling of dopaminergic neurons derived from human embryonic and induced pluripotent stem cells. Stem Cells and Development. 23:4: DOI: 10.1089/scd.2013.0412.

Money KM, Stanwood GD. 2013. Developmental origins of brain disorders: roles for dopamine. Frontiers in Cellular Neuroscience. 7: doi.10.3389/fncel.303.00260. Available from: www.frontiersin.org.

National Center for Biotechnology Information (NCBI) [Internet]. [Updated 2017 Jan 17]. Bethesda, MD: US National Library of Medicine; [cited 2017 Jan 22]. Available from: https://www.ncbi.nlm.nih.gov/gene/111

National Center for Biotechnology Information (NCBI). [Internet]. [Updated 2018 Oct. 2]. Bethesda, MD: US National Library of Medicine; [cited 2012 May]. Available from: https://ghr.nlm.nih.gov/condition/parkinson-disease

Paix A, Folkmann A, Seydoux G. 2017. Precision genome editing Using CRISPR-Cas9 and linear repair templates in C. Elegans. Methods. 122-124: 86-93.

Pickel VM, JOH TH, Reis DJ. 1975. Ultrastructural localization of tyrosine hydroxylase in noradrenergic neurons of the brain. Proc. Nat. Acad. Sci. 72(2):659-663.

Puerto A, Diaz-Hernandez J-I, Tapia M, Gomez-Villafuertes R, Benitez M, Zhang J, Miras-Portugal M, Wandosell F, Diaz-Hernandez M, Garrido J. 2012. Adenylate cyclase 5 coordinates the action of ADP, P2Y1, P2Y13, and ATP-gated P2X7 receptors on axonal elongation. Journal of Cell Sci. 125: 176-188.

R Core Team. (2013). R: A language and environment for statistical computing. R foundation for statistical computing, Vienna, Austria. URL http://www.R-project.org

Rolletschek A, Chang H, Guan K, Czyz J, Meyer M, Wobus AM. 2001. Differentiation of embryonic stem cell-derived dopaminergic neurons is enhanced by survival-promoting factors. Mechanisms of Development. 105: 93-104.

Shaw C, Hisama F, Friedman J, Bird, T/Pagon RA, Adam MP, Ardinger HH, et al. 2015. [Internet]. Seattle (WA): GeneReviews®. [cited 2017 03, 20].

Svenningsson P, Nishi A, Fisone G, Girault JA, Nairn AC, Greengard P. 2004. DARPP-32: an integrator of neurotransmission. Annul Rev Pharmacol Toxicol. 44:269-296.

Willoughby D, Cooper DMF. 2007. Organization and Ca^{2+} Regulation of Adenylyl cyclases in cAMP Microdomains. Physiol. Rev. 87:965 LP-1010.

Uemura T, Ohta Y, Nakao Y, Manaka T, Nakamura H, Takaoka K. 2010. Epinephrine accelerates osteoblastic differentiation by enhancing bone morphogenetic protein signaling through a cAMP/protein kinase A signaling pathway. Bone 47:756-765.

Westenberger S.A, Klein C, Von der Hagen M, Gillessen- Kaesbach G, Munchau A. 2016. Novel adenylate cyclase 5 gene (ADCY5) mutations cause a new phenotype of alternating hemiplegia of childhood (AHC), expanding the clinical spectrum of ADCY5-related hyperkinetic dyskinesias. Neuropediatrics. 47: Vs01-08.

Ye J, Coulouris G, Zaretskaya I, Cutcutache I, Rozen S, Maden T. 2012. Primer-BLAST: A tool to design target-specif ic primers for polymerse chain reaction. BMC Bioinformatics. 13:134.

Zech M, Boesch S, Jochim A, Weber S, Meindl T, Schormair B, Wieland T, Lunetta C, Sansone V, Messner M. 2017. Clinical exome sequencing in early-onset generalized dystonia and large-scale resequencing follow-up. Mov Disord. 32(4): 549-559.

ZEN imaging software (Carl Zeiss Inc, Thornwood, NY).

APPENDICES

Appendix A: CRISPR attempt # 1 revealed mixed sequence results and no c.1252C>T edit made. A. Chromatogram of clone 2B reveals wrong PAM edit (from CCC to GCC). **B.** Chromatogram of clone 2B reveals ambiguous base calling for most of sequence, but detectable wild-type at variant nucleotide (blue highlight).

A). PAM sequence

B). Variant nucleotide

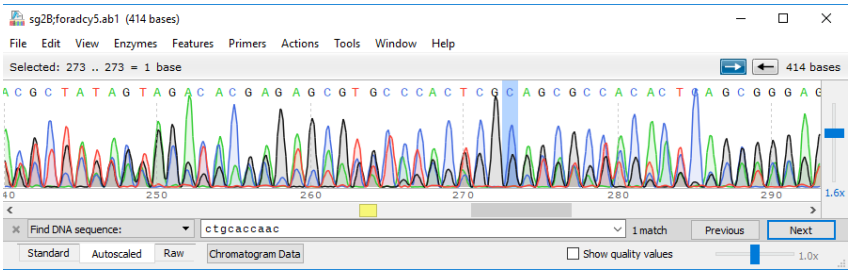

Appendix B: CRISPR attempt # 2 revealed no edit made to variant nucleotide. Example of partial chromatogram of sequence results from CRISPR attempt #2. **A).** Clone # 1 sequence revealed wild-type at variant nucleotide (blue highlight). **B).** Clone # 1 also contained wild-type PAM sequence (blue highlight). **C).** Clone # 2 revealed a c.1252C>G edit (blue highlight). **D)**. Clone # 6 revealed correct PAM edit from CCC to CAC (blue highlight). **E).** Empty-vector transfected control clone revealed wild-type at variant nucleotide (blue highlight). **F).** Empty-vector transfected control clone revealed wild-type at PAM sequence as well (blue highlight).

A).

B).

C).


pcr_sample_1_adcy5;for.ab1 (410 bases)
File Edit View Enzymes Features Primers Actions Tools Window Help
Selected: 206 .. 208 = 3 bases
410 bases
190
200
210
220
230
1.8x
Find DNA sequence:
Previous
Next
Standard
Autoscaled
Raw
Chromatogram Data
Show quality values
1.0x

D).

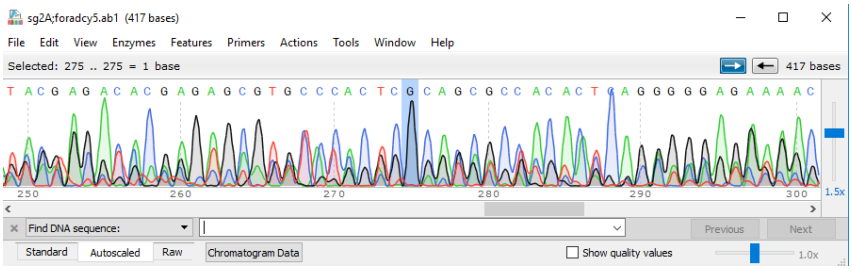
sg2A;foradcy5.ab1 (417 bases)
File Edit View Enzymes Features Primers Actions Tools Window Help
Selected: 275 .. 275 = 1 base
417 bases
250
260
270
280
290
300
1.5x
Find DNA sequence:
Previous
Next
Standard
Autoscaled
Raw
Chromatogram Data
Show quality values
1.0x

E).

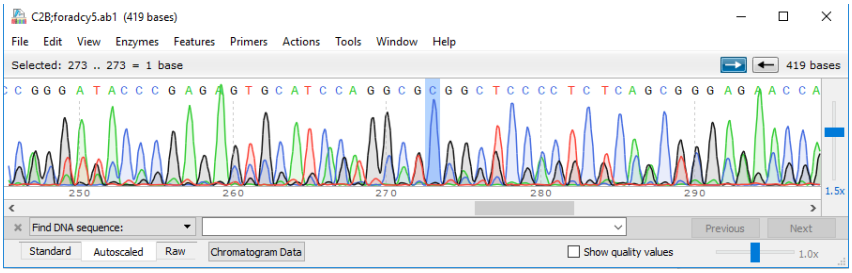
C2B;foradcy5.ab1 (419 bases)
File Edit View Enzymes Features Primers Actions Tools Window Help
Selected: 273 .. 273 = 1 base
419 bases
250
260
270
280
290
1.5x
Find DNA sequence:
Previous
Next
Standard
Autoscaled
Raw
Chromatogram Data
Show quality values
1.0x

F).

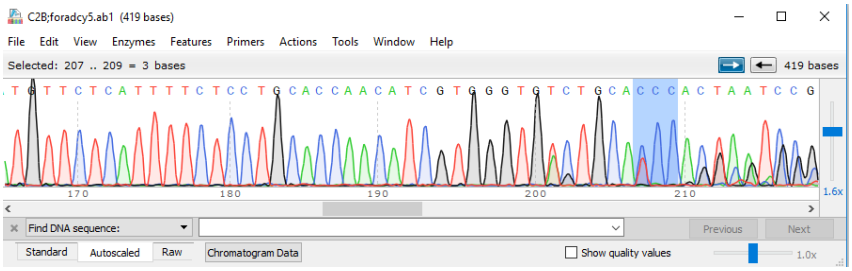
C2B;foradcy5.ab1 (419 bases)
File Edit View Enzymes Features Primers Actions Tools Window Help
Selected: 207 .. 209 = 3 bases
419 bases
170
180
190
200
210
1.6x
Find DNA sequence:
Previous
Next
Standard
Autoscaled
Raw
Chromatogram Data
Show quality values
1.0x

Appendix C: CRISPR attempt # 3 sequence results revealed mixed edits made. Example of partial chromatogram of sequence results from CRISPR attempt #3. **A).** Chromatogram of clone # 4 forward sequence revealed wild-type (blue highlighted C). **B).** Chromatogram of clone # 10 forward sequence revealed c.1252C>A edit (blue highlight), and the reverse sequence reveals c.1252G>T edit (blue highlight). **C).** BLAST analysis of wild-type sequence (query) vs. forward and reverse strand of clone 10 sequence (subject) revealed clone 10 sequence is 98% identical to only a portion of the wild-type sequence.

A).

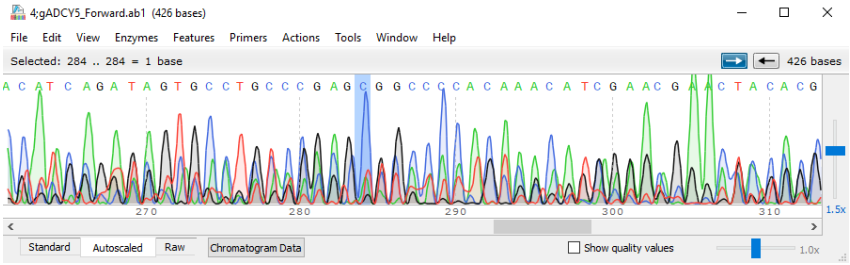

B). Forward

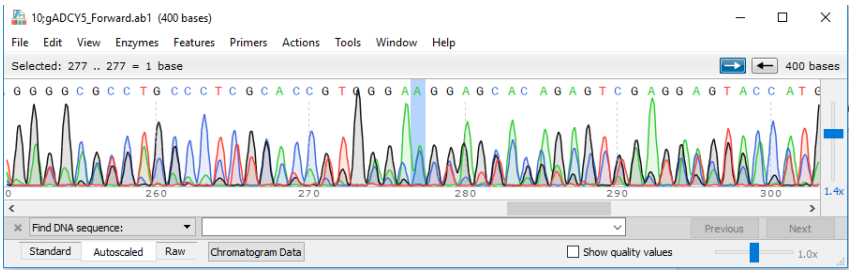

Reverse

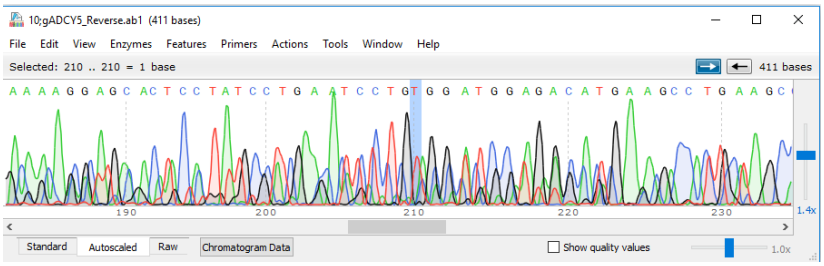

C). Forward strand BLAST

Sequence ID: Query_128991 Length: 400 Number of Matches: 1

Range 1: 18 to 241 Graphics Next Match Previous Match

Score	Expect	Identities	Gaps	Strand
388 bits(210)	1e-112	219/224(98%)	0/224(0%)	Plus/Plus

```
Query  44   TGGTTGGCCGCGTGTGGGGTGCCCTCAGCATTTGTTTGCTAGCGCCAGGTGTGAGTTTGC  103
Sbjct  18   TGNTTGGCCGCGTGTGGGGTGCCCTCAGCATTTGTTTGCTAGCGCCAGGTGTGAGTTTGC  77

Query  104  TGAGACAGGGGCTGAGGGCTTCATGCTTTGGGGCCAGGAAGGTCAGGATCTGAGCTAGGT  163
Sbjct  78   TGAGACAGGGGCTGAGGGCTTCATGCTTTGGGGCCAGGAAGGTCAGGATCTGAGCTAGGT  137

Query  164  GTGCTCCTCTCTCCCTCTGCAGCTTGTCTCCAATGTTCTCATTTTCTCCTGCACCAACAT  223
Sbjct  138  GTGCTCCTCTCTCCCTCTGCAGCTTGTCTCCAATGTTCTCATTTTCTCCTGCACCAACAT  197

Query  224  CGTGGGTGTCTGCACCCACTATCCGGCTGAGGTCTCCCAGAGAC  267
Sbjct  198  CGTGGGTGTCTGCACCCACTATCCCGCTGAGGGCTACCCGAGAC  241
```

D). Reverse strand BLAST

Sequence ID: Query_243233 Length: 411 Number of Matches: 1

Range 1: 15 to 138 Graphics ▼ Next Match ▲ Previous Match

Score	Expect	Identities	Gaps	Strand
215 bits(116)	3e-60	121/124(98%)	0/124(0%)	Plus/Plus

```
Query  43   TCAGCTGAGGTACATCTCAGGGCTCGACTCCGTCCCACTGTGCAAGGGCAGGGGCCTCAC  102
            ||||||||||||||||||||||||||||||||||||||||||||||||||||||||||||
Sbjct  15   TCNGCTGAGGTACATCTCAGGGCTCGACTCCGTCCCACTGTGCAAGGGCAGGGGCCTCAC  74

Query  103  TCACCTGCTGCTGGTTCTCCCGCTGCGAGTGGAGCCGCGCCTGGATGCACTCTCGGGTCT  162
            |||||||||||||||||||||||||||||||||||||||||||||||||| || |||
Sbjct  75   TCACCTGCTGCTGGTTCTCCCGCTGCGAGTGGAGCCGCGCCTGGATGCACTCTCCGGGCT  134

Query  163  CCTG  166
            ||||
Sbjct  135  CCTG  138
```

Appendix D: CRISPR attempt # 3. subcloning of transfected HEK clone #10 reveals mixed alleles A). Forward and Reverse sequence of one subcloned colony reveals a c.1252C>G and c.1252 G>C edit, respectively (blue highlight). **B).** Forward and Reverse sequence of a second subcloned colony reveals wild-type at variant nucleotide (blue-highlight).

A). Forward

Reverse

B). Forward

Reverse

Appendix E: CRISPR attempt # 3 results reveal only one sequence contained correct PAM edit. **A).** Clone # 4 reveals no edit made to PAM (blue highlight). **B).** Clone # 44 contains the silent mutation edit "CCC" to "CAC" (blue highlight).

A).

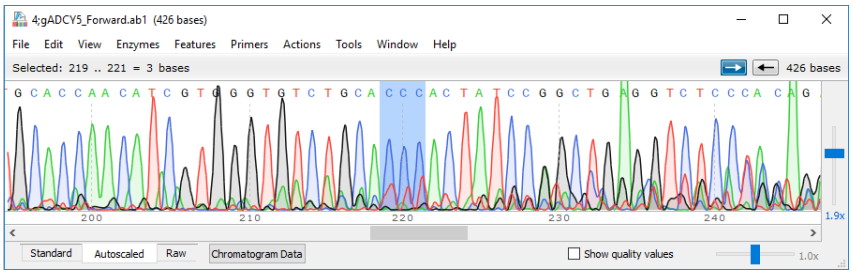

B).

Appendix F: CRISPR attempt # 3. Sequence results of empty- vector-control clone reveal wild-type sequence. A). Control clone # 44 sequence results revealed wild-type sequence at PAM (blue highlight). **B).** Control clone # 44 sequence also revealed wild-type at variant nucleotide (blue highlight), as expected.

A). PAM sequence

B). Variant nucleotide

Appendix G: CRISPR attempt # 4 individual clone PCR confirms correct amplicon size. A). Gel # 1, labeled with clone #'s. L= O'Gene mix ladder. Top row reveals a single amplicon of correct size (441 bp) for most clones, except clone # 5 and # 11. **B).** Gel # 2 reveals all clones have single amplicon of correct size (441 bp). E=empty lane, C= no DNA control (contamination), NT=non-transfected HEK control.

A).

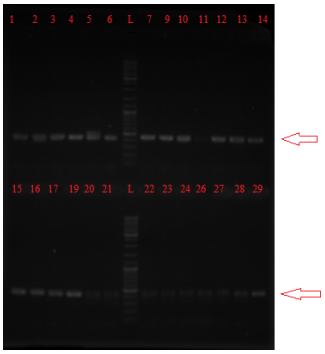

B).

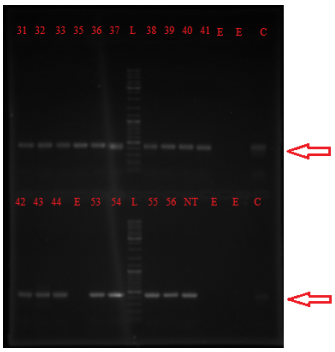

Appendix H: CRISPR attempt # 4 sequence results reveal mixed edits. A). Chromatogram of clone # 33 forward sequence reveals incorrect c.1252C>G edit. **B).** Chromatogram of clone # 29 forward sequence reveals wild-type at variant nucleotide. **C).** Chromatogram of clone #26 forward sequence reveals ambiguous base calling, sequence most likely not monoclonal.

A).

B).

C.


26;foradcy5.ab1 (426 bases)
File Edit View Enzymes Features Primers Actions Tools Window Help
Selected: 37 .. 37 = 1 base
426 bases
260
270
280
290
300
1.9x
Find DNA sequence:
acccgagagt
No matches
Previous
Next
Standard
Autoscaled
Raw
Chromatogram Data
Show quality values
1.0x

Appendix I: CRISPR attempt # 4 sequence results reveal 2 clones with edit c.1252C>T made. A). Clone # 13 sequence, with c.1252C>T edit (blue highlighted T). **B).** Clone # 36 sequence with c.1252C>T edit (blue highlighted T). **C).** BLAST of wild-type (query) vs. clone 13 forward sequence (subject) reveals only 89% identical. **D).** BLAST of wild-type (query) vs. clone 36 forward sequence (subject) reveals 100% identical sequence in only 249 bp of the amplified region.

A).

B).

C).

Sequence ID: Query_193887 Length: 418 Number of Matches: 1

Range 1: 16 to 398 Graphics ▼ Next Match ▲ Previous Match

Score	Expect	Identities	Gaps	Strand
486 bits(263)	5e-142	349/390(89%)	11/390(2%)	Plus/Plus

```
Query  43   GTGGTTG-GCCGCGTGTGGGGTGCCCTCAGCATTTGTTTGCTAGCGCCAGGTGTGAGTTT  101
            ||||||| |||||||||||||||||||||||||||||||||||||||||||||||||||
Sbjct  16   GTGGTTGAGCCGCGTGTGGGGTGCCCTCAGCATTTGTTTGCTAGCGCCAGGTGTGAGTTT  75

Query  102  GCTGAGACAGGGGCTGAGGGCTTCATGCTTTGGGGCCAGGAAGGTCAGGATCTGAGCTAG  161
            ||||||||||||||||||||||||||||||||||||||||||||||||||||||||||||
Sbjct  76   GCTGAGACAGGGGCTGAGGGCTTCATGCTTTGGGGCCAGGAAGGTCAGGATCTGAGCTAG  135

Query  162  GTGTGCTCCTCTCTCCCTCTGCAGCTTGTCTCCAATGTTCTCATTTTCTCCTGCACCAAC  221
            ||||||||||||||||||||||||||||||||||||||||||||||||||||||||||||
Sbjct  136  GTGTGCTCCTCTCTCCCTCTGCAGCTTGTCTCCAATGTTCTCATTTTCTCCTGCACCAAC  195

Query  222  ATCGTGGGTGTCTGCACCCACTATCCGGCTGAGGTCTCCCAGAGACAGGCTTTCCAGGAG  281
            ||||||||||||||||||||||||||||||||||||||||||||||||||||||||||||
Sbjct  196  ATCGTGGGTGTCTGCACCCACTATCCGGCTGAGGTCTCCCAGAGACAGGCTTTCCAGGAG  255

Query  282  ACCCGAGAGTGCATCCA-GGCGCGGCTCCACTCGCAGCGGGAGAACCAGCAGCAGGTGAG  340
            |||||||||||||||| ||| | |||| |||||| |     ||||| || |  ||||
Sbjct  256  ACCCGAGAGTGCATCCAGGGCTCCACTCCCCTCGCAACAACCGAACC--CA-C--GTGAG  310

Query  341  TGAGGCCCCTGCCCTTGCACAGTG-G-GACGGAGTCGAGCCCTGAGATGTACCTCAGCTG  398
            | |||| |||| | | | | | | | | | | | | | | | | | | | | | | | |
Sbjct  311  GGAAGCCACGGCCCTGGC-CT-TGCGCGACGGAATCGAGCCCAGCCATGANATTCACCTG  368

Query  399  AGTGCCTGGCCTAGGGCGGGCAGTGCTTAT  428
            |||| |||||||  ||| |||||||
Sbjct  369  AGTGGATGGCCTAGNCCAGGCCGTGCTTAT  398
```

D).

Sequence ID: Query_137791 Length: 416 Number of Matches: 1

Range 1: 24 to 272 Graphics ▼ Next Match ▲ Previous Match

Score	Expect	Identities	Gaps	Strand
460 bits(249)	3e-134	249/249(100%)	0/249(0%)	Plus/Plus

```
Query  50   GCCGCGTGTGGGGTGCCCTCAGCATTTGTTTGCTAGCGCCAGGTGTGAGTTTGCTGAGAC  109
            |||||||||||||||||||||||||||||||||||||||||||||||||||||||||||
Sbjct  24   GCCGCGTGTGGGGTGCCCTCAGCATTTGTTTGCTAGCGCCAGGTGTGAGTTTGCTGAGAC  83

Query  110  AGGGGCTGAGGGCTTCATGCTTTGGGGCCAGGAAGGTCAGGATCTGAGCTAGGTGTGCTC  169
            |||||||||||||||||||||||||||||||||||||||||||||||||||||||||||
Sbjct  84   AGGGGCTGAGGGCTTCATGCTTTGGGGCCAGGAAGGTCAGGATCTGAGCTAGGTGTGCTC  143

Query  170  CTCTCTCCCTCTGCAGCTTGTCTCCAATGTTCTCATTTTCTCCTGCACCAACATCGTGGG  229
            |||||||||||||||||||||||||||||||||||||||||||||||||||||||||||
Sbjct  144  CTCTCTCCCTCTGCAGCTTGTCTCCAATGTTCTCATTTTCTCCTGCACCAACATCGTGGG  203

Query  230  TGTCTGCACCCACTATCCGGCTGAGGTCTCCCAGAGACAGGCTTTCCAGGAGACCCGAGA  289
            |||||||||||||||||||||||||||||||||||||||||||||||||||||||||||
Sbjct  204  TGTCTGCACCCACTATCCGGCTGAGGTCTCCCAGAGACAGGCTTTCCAGGAGACCCGAGA  263

Query  290  GTGCATCCA  298
            |||||||||
Sbjct  264  GTGCATCCA  272
```

Appendix J: CRISPR attempt # 4. Sequence results reveal PAM edit was not made in any clone sequences. A). Chromatogram of clone # 13 reveals wild-type at PAM sequence (blue highlight). **B).** Chromatogram of clone # 1 reveals wild-type at PAM sequence (blue highlight).

A).

B).

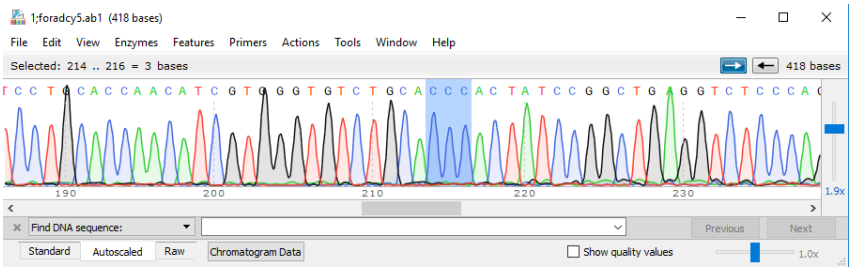

Appendix K: CRISPR attempt # 4 sequence results reveal control clone is wild-type. A). Empty-vector transfection control clone # 53 (replicate 1) reveals wild-type sequence. **B).** Empty-vector transfection control clone # 55 (replicate 2) reveals wild-type sequence. **C).** Non-transfected control HEK cells reveal wild-type sequence. **D).** BLAST analysis of wild-type (query) vs. clone #53 (subject) reveals 99% identical sequence. **E).** BLAST analysis of wild-type (query) vs. clone #55 (subject) reveals 99% identical sequence. **F).** BLAST analysis of wild-type (query) vs. non-transfected HEK cells (subject) reveals 99% identical sequence.

A).

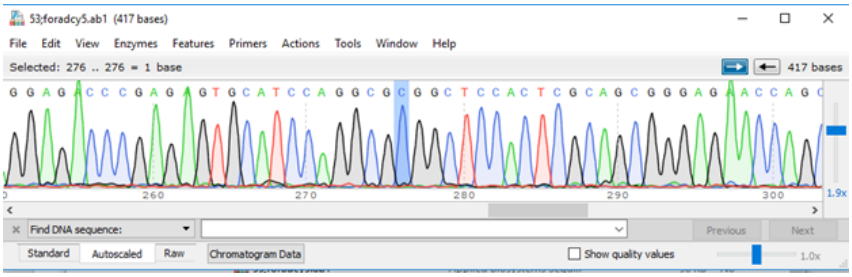

B).

C).

D).

Sequence ID: Query_82071 Length: 417 Number of Matches: 1

Range 1: 15 to 413 Graphics Next Match Previous

Score	Expect	Identities	Gaps	Strand
719 bits(389)	0.0	396/399(99%)	2/399(0%)	Plus/Plus

```
Query  43   GTGGTT-GGCCGCGTGTGGGGTGCCCTCAGCATTTGTTTGCTAGCGCCAGGTGTGAGTTT  101
            ||||||  ||||||||||||||||||||||||||||||||||||||||||||||||||||
Sbjct  15   GTGGTTNAGCCGCGTGTGGGGTGCCCTCAGCATTTGTTTGCTAGCGCCAGGTGTGAGTTT  74

Query  102  GCTGAGACAGGGGCTGAGGGCTTCATGCTTTGGGGCCAGGAAGGTCAGGATCTGAGCTAG  161
            ||||||||||||||||||||||||||||||||||||||||||||||||||||||||||||
Sbjct  75   GCTGAGACAGGGGCTGAGGGCTTCATGCTTTGGGGCCAGGAAGGTCAGGATCTGAGCTAG  134

Query  162  GTGTGCTCCTCTCTCCCTCTGCAGCTTGTCTCCAATGTTCTCATTTTCTCCTGCACCAAC  221
            ||||||||||||||||||||||||||||||||||||||||||||||||||||||||||||
Sbjct  135  GTGTGCTCCTCTCTCCCTCTGCAGCTTGTCTCCAATGTTCTCATTTTCTCCTGCACCAAC  194

Query  222  ATCGTGGGTGTCTGCACCCACTATCCGGCTGAGGTCTCCCAGAGACAGGCTTTCCAGGAG  281
            ||||||||||||||||||||||||||||||||||||||||||||||||||||||||||||
Sbjct  195  ATCGTGGGTGTCTGCACCCACTATCCGGCTGAGGTCTCCCAGAGACAGGCTTTCCAGGAG  254

Query  282  ACCCGAGAGTGCATCCAGGCGCGGCTCCACTCGCAGCGGGAGAACCAGCAGCAGGTGAGT  341
            ||||||||||||||||||||||||||||||||||||||||||||||||||||||||||||
Sbjct  255  ACCCGAGAGTGCATCCAGGCGCGGCTCCACTCGCAGCGGGAGAACCAGCAGCAGGTGAGT  314

Query  342  GAGGCCCCTGCCCTTGCACAGTGGGACGGAGTCGAGCCCTGAGATGTACCTCAGCTGAGT  401
            ||||||||||||||||||||||||||||||||||||||||||||||||||||||||||||
Sbjct  315  GAGGCCCCTGCCCTTGCACAGTGGGACGGAGTCGAGCCCTGAGATGTACCTCAGCTGAGT  374

Query  402  GCCTGGCCTAGGGCGGGCAGTGCTTATTACGGCT-GCCA  439
            ||||||||||||||||||||||||||||||||| ||||
Sbjct  375  GCCTGGCCTAGGGCGGGCAGTGCTTATTACGGCTTGCCA  413
```

E).

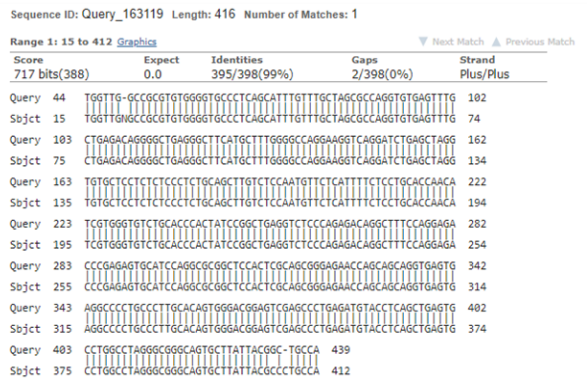

Sequence ID: Query_163119 Length: 416 Number of Matches: 1

Range 1: 15 to 412 Graphics ▼ Next Match ▲ Previous Match

Score	Expect	Identities	Gaps	Strand
717 bits(388)	0.0	395/398(99%)	2/398(0%)	Plus/Plus

```
Query  44   TGGTTG-GCCGCGTGTGGGGTGCCCTCAGCATTTGTTTGCTAGCGCCAGGTGTGAGTTTG  102
            |||||| |||||||||||||||||||||||||||||||||||||||||||||||||||||
Sbjct  15   TGGTTGNGCCGCGTGTGGGGTGCCCTCAGCATTTGTTTGCTAGCGCCAGGTGTGAGTTTG  74

Query  103  CTGAGACAGGGGGCTGAGGGCTTCATGCTTTGGGGCCAGGAAGGTCAGGATCTGAGCTAGG  162
            ||||||||||||||||||||||||||||||||||||||||||||||||||||||||||||
Sbjct  75   CTGAGACAGGGGGCTGAGGGCTTCATGCTTTGGGGCCAGGAAGGTCAGGATCTGAGCTAGG  134

Query  163  TGTGCTCCTCTCTCCCTCTGCAGCTTGTCTCCAATGTTCTCATTTTCTCCTGCACCAACA  222
            ||||||||||||||||||||||||||||||||||||||||||||||||||||||||||||
Sbjct  135  TGTGCTCCTCTCTCCCTCTGCAGCTTGTCTCCAATGTTCTCATTTTCTCCTGCACCAACA  194

Query  223  TCGTGGGTGTCTGCACCCACTATCCGGCTGAGGTCTCCCAGAGACAGGCTTTCCAGGAGA  282
            ||||||||||||||||||||||||||||||||||||||||||||||||||||||||||||
Sbjct  195  TCGTGGGTGTCTGCACCCACTATCCGGCTGAGGTCTCCCAGAGACAGGCTTTCCAGGAGA  254

Query  283  CCCGAGAGTGCATCCAGGCGCGGCTCCACTCGCAGCGGGAGAACCAGCAGCAGGTGAGTG  342
            ||||||||||||||||||||||||||||||||||||||||||||||||||||||||||||
Sbjct  255  CCCGAGAGTGCATCCAGGCGCGGCTCCACTCGCAGCGGGAGAACCAGCAGCAGGTGAGTG  314

Query  343  AGGCCCCTGCCCTTGCACAGTGGGACGGAGTCGAGCCCTGAGATGTACCTCAGCTGAGTG  402
            ||||||||||||||||||||||||||||||||||||||||||||||||||||||||||||
Sbjct  315  AGGCCCCTGCCCTTGCACAGTGGGACGGAGTCGAGCCCTGAGATGTACCTCAGCTGAGTG  374

Query  403  CCTGGCCTAGGGCGGGCAGTGCTTATTACGGC-TGCCA  439
            ||||||| |||||||||||||||||||||||| | |||||
Sbjct  375  CCTGGCCTAGGGCGGGCAGTGCTTATTACGCCCTGCCA  412
```

F).

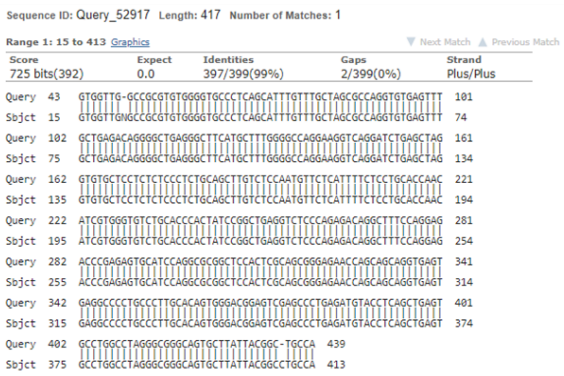

Sequence ID: Query_52917 Length: 417 Number of Matches: 1

Range 1: 15 to 413 Graphics ▼ Next Match ▲ Previous Match

Score	Expect	Identities	Gaps	Strand
725 bits(392)	0.0	397/399(99%)	2/399(0%)	Plus/Plus

```
Query  43   GTGGTTG-GCCGCGTGTGGGGTGCCCTCAGCATTTGTTTGCTAGCGCCAGGTGTGAGTTT  101
            ||||||| |||||||||||||||||||||||||||||||||||||||||||||||||||
Sbjct  15   GTGGTTGNGCCGCGTGTGGGGTGCCCTCAGCATTTGTTTGCTAGCGCCAGGTGTGAGTTT  74

Query  102  GCTGAGACAGGGGGCTGAGGGCTTCATGCTTTGGGGCCAGGAAGGTCAGGATCTGAGCTAG  161
            ||||||||||||||||||||||||||||||||||||||||||||||||||||||||||||
Sbjct  75   GCTGAGACAGGGGGCTGAGGGCTTCATGCTTTGGGGCCAGGAAGGTCAGGATCTGAGCTAG  134

Query  162  GTGTGCTCCTCTCTCCCTCTGCAGCTTGTCTCCAATGTTCTCATTTTCTCCTGCACCAAC  221
            ||||||||||||||||||||||||||||||||||||||||||||||||||||||||||||
Sbjct  135  GTGTGCTCCTCTCTCCCTCTGCAGCTTGTCTCCAATGTTCTCATTTTCTCCTGCACCAAC  194

Query  222  ATCGTGGGTGTCTGCACCCACTATCCGGCTGAGGTCTCCCAGAGACAGGCTTTCCAGGAG  281
            ||||||||||||||||||||||||||||||||||||||||||||||||||||||||||||
Sbjct  195  ATCGTGGGTGTCTGCACCCACTATCCGGCTGAGGTCTCCCAGAGACAGGCTTTCCAGGAG  254

Query  282  ACCCGAGAGTGCATCCAGGCGCGGCTCCACTCGCAGCGGGAGAACCAGCAGCAGGTGAGT  341
            ||||||||||||||||||||||||||||||||||||||||||||||||||||||||||||
Sbjct  255  ACCCGAGAGTGCATCCAGGCGCGGCTCCACTCGCAGCGGGAGAACCAGCAGCAGGTGAGT  314

Query  342  GAGGCCCCTGCCCTTGCACAGTGGGACGGAGTCGAGCCCTGAGATGTACCTCAGCTGAGT  401
            ||||||||||||||||||||||||||||||||||||||||||||||||||||||||||||
Sbjct  315  GAGGCCCCTGCCCTTGCACAGTGGGACGGAGTCGAGCCCTGAGATGTACCTCAGCTGAGT  374

Query  402  GCCTGGCCTAGGGCGGGCAGTGCTTATTACGGC-TGCCA  439
            ||||||| |||||||||||||||||||||||| | |||||
Sbjct  375  GCCTGGCCTAGGGCGGGCAGTGCTTATTACGGCCTGCCA  413
```